BUREAU OF MINERAL RESOURCES, GEOLOGY AND GEOPHYSICS

RECORD

RECORD 1988/9

Hydrothermal Transport of Platinum and Gold in the Unconformity-related Uranium deposits: A Preliminary Thermodynamic Investigation.

by

Subhash Jaireth

BUREAU OF MINERAL RESOURCES,
GEOLOGY AND GEOPHYSICS

RECORD 1988/9

Hydrothermal Transport of Platinum and Gold in the Unconformity-related Uranium deposits: A Preliminary Thermodynamic Investigation.

* Important features of the Unconformity-related deposits.

* Solubility, Transport and deposition of Platinum.

* Solubility, Transport and deposition of Gold.

* Application to the genesis of PGE-Au concentrations in the unconformity-related deposits.

Subhash Jaireth
University of Roorkee, Roorkee, India.

March 1988

CONTENTS

Acknowledgements

This work was undertaken on the suggestion of Chris Heinrich and was completed under his guidance. I am very grateful to him for helping me understand the various intricacies involved in using the CSIRO-SGTE THERMODATA SYSTEM. Discussion with Mike Solomon, Dick Henley, Neville Higgins, Stuart Needham and Hashem Etminan were of a great help in completing this work. I am grateful to the Director B.M.R and the Chief, Division of Petrology and Geochemistry for hosting me during my fellowship period and providing me all the facilities. Finally, I would like to thank the Ministry of Human Resources Development, Government of India for awarding me the National fellowship to undertake research at the Bureau of Mineral Resources, Canberra.

Introduction

During the last 20 years the possibility of hydrothermal transport of platinum group elements (PGE) has attracted considerable attention. Signs of hydrothermally deposited and/or redeposited PGE minerals have been reported from many known copper-nickel deposits associated with basic-ultrabasic intrusives from South Africa (Mihalik et al 1974, Tarkian and Stumpfl, 1975, Peyrel, 1984) , Finland (Hakli et al, 1976, Pispanen and Tarkian,1986) and U.S.S.R (Yusko-Zakharova et al 1967). In some copper porphyry deposits variable but anamolous Pt and Pd concentrations have been reported from China(Yang et al,1974) and Armenia, U.S.S.R (Faramazyan et al,1975).

The possibility of hydrothermal transport of PGE in relatively low temperature ore fluids was indicated by Otteman and Augustithis (1987) who discussed the mineralogy and genesis of platinum bearing nuggets from lateritic cover over ultrabasic rocks in W.Ethopia. Fuchs and Rose (1974) have drawn attention to the behaviour of platinum and palladium during weathering and have discussed the relative mobility of these two elements in the soil profile. High PGE concentration of probable hydrothermal origin was reported by Kucha (1982) in the Polish Kupferschiefer where it contains up to 700 ppm Pt, 400 ppm Pd, 600 ppm Ir and 1100 ppm Au. The latest in this series of hydrothermal occurrences of PGE are the unconformity related uranium deposits of South Alligator River valley (Needham, 1987). The ores in a few of the unconformity related deposits in Athabasca basin of Canada (e.g. Midwest) are also reported to contain minor concentrations of gold and PGE (Wray, 1987).

In spite of so many known possible hydrothermal occurrences of PGE, except for an abstract by Mountain et al (1986), no serious attempt has yet been made to evaluate thermodynamically the possibility of transporting PGE in ore fluids. Westland (1981), Bowles (1986) and Brookins(1987) have presented a number of Eh-pH diagrams at 25°C and discussed behaviour of

platinum in near-surface fluids. In the present study an attempt has been made to evaluate the possibility of hydrothermal transport of platinum and gold in subcritical aqueous solutions at temperatures between 25 and 250°C. Calculations have been carried out based on the available basic thermodynamic data on the aqueous species of platinum and gold. This preliminary study is primarily aimed to evaluate transport and depositional mechanisms of platinum and gold in environments related to the unconformity type uranium deposits of the Northern Territory, including the Coronation Hill deposit.*

* During the final phase of completion of this study, an abstract by Wilde et al (1988) based on an independent but similar study was submitted to the Bicentenial Gold '88 Symposium and was part of a Ph.D thesis submitted in January 1988 by A.Wilde.

Important Features of the Unconformity-Related Uranium deposits

There is very little information available on the nature of gold and PGE concentration in the unconformity- related uranium deposits, though the close spatial association between uranium and gold-PGE mineralizations has been stressed by Needham (1987). The geology of the unconformity- related uranium deposits on the other hand is extensively documented. The characteristic features of these deposits, as summarized in Table1, is briefly discussed below.

1. The deposits occur close to an unconformity between rock formations, different in age and lithology (Dahlkamp, 1978, Hoeve and Sibbald, 1978a, Hegge et al. 1980).

2. The older rocks below the unconformity are usually represented by various metamorphosed and/or unmetamorphosed sedimentary rocks marked by relatively high concentrations of carbonaceous material in one or few members. In many deposits lithological control of mineralization by carbonaceous metasediments is very evident though in others such a control is not so obvious (Ayers and Eadington, 1975, Hoeve and Sibbald, 1978a).

3. The younger rocks overlying the unconformity are generally represented by terrestrial clastic sedimentary (sandstone, conglomerate etc.) and/or volcanic rocks. Based on sedimentological characteristics, Ramaekers (1977) has indicated that the depositon of Athabasca sandstone formation took place in a shallow-water braided-stream enviornment. Hoeve and Sibbald (1978b) described extensive hematite staining with substantial concentration of ferric oxide in the coarse basal units of this formation. According to them, conditions during deposition and/or diagenesis must have been generally oxidizing. The unconformity in some of the regions is marked by the presence of a regolith of deeply weathered hematite-stained rock, mineralogically and chemically similar to recent laterites (Hoeve and Sibbald, 1978b).

4. The bulk of the U-PGE-Au mineralization is located immediately below the unconformity in fractured and altered rocks and also immediately above the unconformity in sandstones and conglomerates.

5. In many deposits structural control of mineralization is conspicuous e.g, where minerals are concentrated in fractured and brecciated rocks close to fault zones (Dahlkamp, 1978, Hoeve and Sibbald,1978a, Wray, 1986)

6. Uranium mineralization in these deposits is accompanied by Ni, As, Co, Au-Ag and PGE mineralization. Gold and PGE mineralization at Coronation Hill are thought to be coeval processes and show close spatial association with the

TABLE 1
Characteristic features of Unconformity - type Uranium deposits

	Jabiluka & Nabarlek[1]	South Alligator River deposits[3,4,5] including Coronation Hill deposit	Key Lake[6]	Rabbit Lake[8]	Mid West[10]
Rocks below unconformity	Mica and quartz feldspar schist and gneiss, lower members calcareous and carbonaceous, para amphibolites, dolomite magnesite rock. (Cahil Formation) Lower Proterozoic.	Carbonaceous shales, Ferruginous siltstone, dolomite (Koolpin Formation)	Graphitic quartz biotite-plagioclase. cordierite gneiss. (Aphebian)	metapelites (commonly graphitic), quartzites,meta-arkoses, feldspar granulites, calc-silicates - (Wollaston Group).	Biotite-garnet-feldspar gneiss with sillimanite or cordierite rich bands, graphitic gneiss
Rocks above unconformity	Sandstone, conglomerate (Kombolige formation - M. Proterozoic)	Sandstone, Conglomerate, Rhyolite, ignimbrite, tuff. Quartz-greywacke volcanics, basalt (Kombolgie formation formation Edith River volcanics).	Sandstone, at the base conglomeratic. (Athabasca).	Sandstone, conglomerate, shale, subgreywacke (Athabasca).	Quartz sandstone, conglomerate, silt, clay, hematized mudstone.
Host rocks	Chlorite and or graphite schist and brecciated equivalents.	Ferruginous siltstone, carbonaceous shales, sandstone, rhyolites	Kaolinite mylonite, chlorite myolinite, Graphitic schist, Quartzite (fragments of Athabasca sandstone).	Altered calcareous metasedimentaries, sandstone.	Graphitic horizons of metasedimentaries, sericitic /hematitic body of mudstone, sandstone.
Ore localizing factors	Lithological-chlorite and/or graphite schist.	Lithological-carbonaceous bearing rocks. Structural-fault zone.	Lithological-(Locally graphitic). Structural-Fault zones mylonitized and brecciated rocks.	Lithological-Chloritized rocks and graphitic metasediments. Structural-faults.	Lithological-graphitic horizons. Structural-Faults.
Ore minerals.	pitchblence, coffinite, brannerite; sulphides.	pitchblende, secondary minerals of uranium, sulphides.	Pitchblence, sooty pitchblende; coffinite, Ni-Arsenides, sulphides.	Pitchblende-I, pitchblende-II, coffinite; hematite, sulphides, sulphides, native copper, Mo-Co.	Pitchblende-I, pitchblende-II, coffinite, sulphides, Ni-Arsenides, hematite. Traces of PGE.
Gangue minerals.	Chlorite, quartz, sericite.	red and grey chert, siderite, vein quartz.	Kaolinite, chlorite, siderite, calcite, sphene, epidote.	Quartz, dravite, dolomite, siderite, chlorite, calcite.	Siderite, dolomite, calcite, sericite, chlorite.
Temperature,pressure and compositiion of fluids	85°-260° (Stable isotopes)[2] 75°-160°C (Fluid inclusion) 500 to 250-350 bars. 20-30wt% $NaCl+CaCl_2+MgCl_2$		137°C deposition of pitchblende	180-225°C, 160±10°C[9], 750±150 bars, 30 wt% eq. NaCl	
Mineralization other than uranium	Au, P.G.E.	Au, P.G.E.		Ni, Co (minor)	Ni, A, Co, Au, Pt
Age of mineralization	800-900 my (Kombolgie Formation 1600 my)	815-710 my	1350+4 my, 200 my younger than the Manitou Falls of Athabasca group.	1780+20 my, 1125+25 my (younger than the Athabasea group rocks	1200-1300 my (Age of Athabasea rocks 1450+30my).

1. Hegge et al (1980)
2. Ypma and Fuzikawa (1980)
3. Ayres and Eadington (1975)
4. Needham (1987)
5. Needham and Stuart-Smith (1987)
6. Dahlkamp (1978)
7. Trocki et al (1984)
8. Hoeve and Sibbald (1978)
9. Pagel et al (1980)
10. Wray et al (1986)

uranium mineralization. However the temporal relationship between the Au-PGE and uranium mineralizations is not very clear (Needham, 1987).

7. Published data on the ages of initial mineralization clearly shows that the mineralization was younger than the depositon of rocks overlying the unconformity surface (Hoeve and Sibbald, 1978a, Trocki et al. 1984, Maas et al., 1987).

8. Fluid inclusion studies in quartz thought to be associated with the mineralization indicate high salinity, chloride-rich fluids with temperatures varying between 160 and 225°C (Pagel et al. 1980, Ypma and Fuzikawa, 1980).

Solubility, Transport and Deposition of Platinum

Source of Thermodynamic Data

The PGE form stable planar (PGE as bivalent) and octahedral (PGE as tetravalent) complexes with different ligands (halides, hydroxyl, amine etc.). Their chemistry has been reviewed by Westland (1981). Basic thermodynamic data (enthalpy, entropy and Gibbs free-energy of formation) is available only for a few aqueous species of platinum. Goldberg and Hepler(1968) have reported stability data at 25°C for a number of aqueous species of platinum, which forms the basis of the compilations by Wagman et al (1969) and Westland (1981). In the present study, out of all the halide complexes of platinum, only chloro-complexes were considered, because only they are likely to be geologically more important than bromide and iodide complexes. In addition to $PtCl_4^{-2}$ and $PtCl_6^{-2}$,data on one ammonia and two chloro-ammonia complexes of platinum have been also been used for calculations. Mean heat capacities of the above mentioned five aqueous species of platinum were calculated using the method of Criss-Cobble (1964) outlined in the C.S.I.R.O - SGTE THERMODATA system of Turnbull and Wadsley (1986). Table 2 summarizes basic thermodynamic data for these species used in these calculations. The stability data for solid PtS and PtS_2 was taken from Goldberg and Hepler (1968), while data for most of the gaseous and solid species were obtained from the data banks CPDMRLDATA and CPDNBSDATA. Sources for the stability data for other aqueous and solid species have been summarized in table 3.

Table 2 Thermodynamic Data at 25°C for Aqueous Species of Platinum

Aqueous complex	H_f^o cal/mole	S^o cal/deg.mole	Cp* Cal/K	G_f^o cal/mole
$PtCl_4^{-2}$	-119312	37.046	-81.770	-86309
$PtCl_6^{-2}$	-159704	52.510	-82.210	-115423
$Pt(NH_3)Cl_3^{-1}$	-110889	47.084	-81.630	-72706
$Pt(NH_3)_3Cl^+$	-94694	27.008	45.590	-34149
$Pt(NH_3)_4^{+2}$	-86496	10.038	-62.430	-12708

* mean heat capacities calculated using method of Criss and Cobble (1968)

Table 3. Source of Stability data for species used in the calculations

Species	Source
a) Solid	
$Al_2Si_2O_5(OH)_4$	Helgeson (1969)
b) Aqueous	
H_2	Drummond(1981)
O_2	Naumov et al. (1971)
N_2	Giggenbach(1980)
NH_3	Cobble et al (1982)
CO_2	Drummond (1981)
CH_4	Drummond (1981)
H_2S	Drummond (1981)
HS^-	Cobble et al (1982)
HSO_4^-	Murray and Cubicciotti (1983)
SO_4^{-2}	Cobble et al (1982)
HCO_3^{-1}	Cobble et al (1982)
CO_3^{-2}	Cobble et al (1982)
H_4SiO_4	Cobble et al (1982)
K^+	Cobble et al (1982)
Na^+	Cobble et al (1982)
Fe^{+2}	Cobble et al (1982)
Cl^-	CPDMRLDATA
OH^-	Cobble et al (1982)
HCl	Henley et al. (1984)
KCl	SOLTHERHM, Reed (1986)
NaCl	SOLTHERHM, Reed (1986)
KOH	SOLTHERHM, Reed (1986)
NaOH	SOLTHERHM, Reed (1986)
$FeCl^+$	Ruaya (1986)

Speciation of Aqueous Platinum in the System Pt-N-Cl-O-H(-S)

a) Predominance diagrams

In order to study the speciation of aqueous species of platinum a series of log f_{H_2} - pH diagrams at fixed temperature were calculated. The first series of these diagrams (Fig 1) shows the predominance areas of aqueous platinum species at very low concentrations of platinum i.e. in solutions that are undersaturated with solid platinum phases. These calculations show that, $PtCl_4^{-2}$ (aq) has a wide predominance field in oxidized solutions at all temperatures. $PtCl_6^{-2}$ (aq) is stabilized under even lower f_{H_2} and/or very acidic conditions. Also plotted on these diagrams are the fields of predominance of three aqueous species of nitrogen, NH_3, N_2 and NH_4^+. Nitrogen bearing species of platinum are dominant only at relatively high f_{H_2} (below hematite+magnetite line), where reduced nitrogen ligands NH_3 and NH_4^+ become stable in appreciable amounts. The second series of these diagrams (Figs. 2 and 3) has been calculated with higher activities of dissolved platinum in the system to depict solubility contours for metallic platinum and the platinum sulfides. Thus, even at a low concentration of 0.01 ppb of total dissolved platinum, fields of predominance of nitrogen bearing aqueous species of platinum are displaced by native platinum or sulfides of platinum. The only stable aqueous species of platinum are the chloro species. The effect of total dissolved chloride in the system can be seen on Fig 2a and 2c where 0.01 ppb contour for $PtCl_4^{-2}$ (aq) have been plotted at two different activities of total chloride (0.02 and 2.0) in the system. As expected a decrease in the activity of total chloride narrows down the field of $PtCl_4^{-2}$ (aq) and the contours move towards lower f_{H_2} (higher redox state) conditions. Equilibrium constants of some important reactions involving aqueous species of platinum and used in these calculations have been summarized in table 4.

Table 4 Calculated Equilibrium Constants of Some Important reactions

Reaction	Equilibrium constant (logK)			
	25°C	100°C	200°C	250°C
1. $Pt + 6Cl^-(aq) + O_2(g) + 4H^+ = PtCl_6^{-2}(aq) + 2H_2O$	29.8	21.84	16.71	15.39
2. $Pt + 4Cl^-(aq) + 1/2O_2(g) = PtCl_4^{-2}(aq) + H_2O$	12.59	8.85	6.16	5.418
3. $Pt + 3Cl^-(aq) + 1/2N_2(aq) + 1/2H_2O = Pt(NH_3)Cl_3^-(aq) + 1/4O_2(g)$	-33.39	-27.7	-23.23	-21.70
4. $Pt + Cl^-(aq) + 3/2N_2(aq) + 7/2H_2O + 2H^+ = Pt(NH_3)_3Cl^+(aq) + 7/4O_2(g)$	-134.30	-108.7	-87.94	-80.78
5. $Pt + 5H_2O + 2N_2(aq) + 2H^+ = Pt(NH_3)_4^+(aq) + 5/2O_2(g)$	-186.30	-151.0	-122.8	-113.2

In order to investigate the effect of temperature, a number of log f_{O2} - 1/T diagrams have been calculated (Figs 4, 5). The speciation of aqueous species of platinum has been calculated for activities of total dissolved chloride and nitrogen equal to 2 and 1 respectively. The pH of the fluid has been buffered by the Kmq(potash feldspar+muscovite+quartz) assemblage at three different activities of dissolved potassium (1, 0.1 and 0 .01). In the first series of these diagrams (Fig 4) speciation has been calculated for solutions undersaturated with solid platinum phases while in Fig 5 solid platinum and sulfides of platinum have been introduced in the system and the boundaries between the fields of solid platinum phases and aqueous species of platinum have been drawn for 0.01 ppb of dissolved platinum which is equal to the lowest concentration for any geologically realistic transport of platinum in aqueous solutions. $PtCl_4^{-2}$ (aq) and $PtCl_6^{-2}$ (aq) are the only two stable aqueous species that limit the solubility of platinum. The diagrams show that even at a very high chloride activity (a_{Cl} = 2) and probably higher than realistic potassium activity (a_K=1), very oxidizing conditions, well above the hematite+magnetite buffer and close to or above the Mn_3O_4+Mn_2O_3 buffer are required for any geologically realistic transport of platinum in aqueous solutions.

b) Amine complexes

Under equilibrium conditions, N-bearing platinum complexes are unlikely to contribute to platinum transport in low- to moderate-temperature geological systems since they do not have a predominance field despite the high total activity of nitrogen species of 1 assumed in the calculations of Fig. 2. This is understandble because the higher oxidizing conditions required to stabalize aqueous Pt(II) and Pt(IV) will thermodynamically de-stabilize the reduced amine ligands NH_3 and NH_4^+ . The highest contribution of amine complexes to the equilibrium solubility of platinum is expected to occur at f_{O2}/pH conditions near the "triple point" of equal activities of NH_3(aq), NH_4^+(aq) and N_2(aq) (point T in Figs. 1a to 1d). Fig 6 shows the contribution of all platinum

complexes to the solubility of elemental platinum at this "triple point", as a function of temperature. Although N-bearing complexes do predominate under these conditions, their activity of 10^{-20} or less is clearly too low for geologically realistic transport of platinum.

Rock Buffered Solubility of Platinum

Fig 7 represents the solubility of platinum in rock buffered conditions where pH of the fluid is buffered by the Kmq assemblage while f_{O2} is buffered by the magnetite+hematite pair. In all such fluids solubility increases with temperature with $PtCl_4^{-2}$ (aq) becoming dominant at higher temperatures. The solubility also increases with decrease in pH but in all such rock buffered fluids, solubility is very low (activity of dissolved species less than 10^{-20} at all temperatures).

When the fluid is buffered at higher f_{O2} conditions by a $Mn_3O_4+Mn_2O_3$ assemblage (Fig 8) the solubility of platinum increases to geologically realistic values of 0.03 ppb at 25°C and 0.5 ppb at 250°C. In such fluids, the solubility increases with temperature and decreases with increase in pH, with chloro-complexes clearly being the dominant aqueous species.

Solubility of Platinum in Saline Fluids Containing Atmospheric O_2

In order to investigate the possibility of transporting platinum in saline, surface derived waters (see discussion below), the solubility of platinum in fluids saturated with atmospheric oxygen was calculated. Calculations have been carried out under conditions where the pH of the fluid is buffered by the Kmq assemblage and are aimed to model conditions where a surface brine, originally saturated with air at 25°C is heated in contact with a rock containing an excess of Kmq assemblage but no solid redox buffers. Fig. 9 shows the solubility of platinum in such a fluid with different activities of chloride and potassium(pH). Thus a fluid saturated with atmospheric oxygen and buffered by the Kmq assemblage (a_{Cl}=1, a_K= 0.01) can dissolve at 25°C, upto 60 ppm of platinum as chloro-complexes. Under these conditions

solubility increases slightly with increase in the activity of chloride and potassium(decrease in pH), but surprisingly decreases with rise in temperature. Fig 10 represents the solubility of platinum in a fluid saturated with atmospheric oxygen with pH buffered by the Kcq (potash feldspar+kaolinite+quartz) assemblage.

Possible Mechanisms of Deposition of Platinum

From the previous caculations it is clear that the solubility of platinum in a saline fluid at a fixed temperature and pH depends mainly on the redox state of the fluids. Lowering of f_{O2} triggers a drastic fall in the solubility. Calculations have been carried out to evaluate the reaction of an acid, saline fluid, initially at high redox state (saturated with atmospheric oxygen or buffered by the Mn_3O_4+Mn_2O_3 assemblage) with a reducing agent (graphite or magnetite).

Figs. 11a and 11b represent changes in the activity of dissolved platinum as saline (a_{Cl} = 1, a_K = 0.01), platinum-bearing fluid initially saturated with atmospheric oxygen starts reacting with magnetite and graphite at 100°C respectively. Fig 12 represents the reaction of a similar platinum-bearing fluid, initially buffered by the Mn_3O_4+Mn_2O_3 assemblage, with magnetite at 250°C. These calculation show that reaction with small amount of reducing agent can cause precipitation of the total dissolved platinum in the fluids. In addition to graphite and magnetite, other Fe^{+2} bearing minerals (sulfides and silicates) can also cause precipitation. Additionally, mixing of the highly oxidized platinum-bearing fluids with relatively more reduced fluids (containing CH_4, H_2S etc.) of deeper origin can also cause precipitation of platinum.

Discussion and conclusions

Our calculations on the stability of aqueous species of platinum in the system Pt-Cl-N-O-H(-S) suggests the following :

1. Of all the known aqueous species of platinum for which basic thermodynamic data is available, chloro species namely $PtCl_4^{-2}$ and $PtCl_6^{-2}$, are the only species that could possibly contribute to the hydrothermal transport of plainum in subcritical fluids of geologically realistic origin. Amine and other nitrogen-bearing complexes are unable to account for more than 10^{-20} m/Kg of dissolved platinum and hence are not important for the transport of platinum in natural crustal fluids.

2. The equilibrium solubility of platinum is primarily controlled by redox conditions and geologically realistic transport of platinum as chloro-complexes requires unusally oxidized chloride-rich fluids. In fluids buffered with regard to redox by the magnetite+hematite assemblage, solubility of platinum only reaches a maximum of 0.6×10^{-19} m/Kg at 250°C. In similar fluids but buffered by $Mn_3O_4+Mn_2O_3$ assemblage the solubility increases upto 1 ppb whereas in air saturated fluids as much as 60 ppm of platinum can be dissolved at 25°C. It can be concluded that transport of platinum in the form of known platinum complexes cannot be effected by any common "deep" hydrothermal fluids such as igneous, metamorphic or even a typically geothermal/epithermal fluid, all of which are typically at a reduced redox state buffered by the equilibria between Fe^{+2} and Fe^{+3} minerals or $Fe^{+2}(aq)$ complexes, with f_{O2} generally near or below the hematite + magnetite buffer. If platinum is ever transported in ore-forming concentrations by any such reducing fluid, extremely stable (yet experimentally untested) platinum complexes are required. By analogy with the chemistry of gold, Pt(II)-bisulfide complexes are a likely possibility (Mountain et al. 1986).

3. The only geologically realistic fluids that are potentially capable of transporting platinum in the form of the known chloro-complexes are the chloride brines with a high redox state that is more or less directly influenced by atmospheric oxygen. These could be saline groundwaters or possibly seawater, buffered by the oxidized phases of the surface , subsurface or sea-floor weathering regime, where the manganese oxide minerals (e.g. $Mn_3O_4+Mn_2O_3$) buffer redox state at a higher level. Such chloride-rich fluids can easily transport upto 1ppb of platinum at 250°C (Fig 8). Alternatively, a saline fluid with a direct atmospheric contribution of oxygen would provide a good transporting agent for platinum in the form of chloro-complexes at all temperatures (Figs 9 and 10).

Solubility, Transport and Deposition of Gold

In the unconformity-related uranium deposits, PGE mineralization shows a close spatial and temporal association with gold mineralization. In this study the geochemical behaviour of gold has been investigated to evaluate if the highly oxidized, saline and acidic fluids that are capable of transporting platinum can also transport significant amounts of gold and whether mechanisms such as reduction by carbonaceous material and magnetite which are effective in depositing platinum, can also deposit gold.

Basic stability data for aqueous chloro-complexes of gold, $AuCl_4^-$ and $AuCl_2^-$ have been taken from Helgeson (1969) which like the data on Pt-species are extrapolated from 25°C data. The stability data for aqueous $Au(HS)_2^-$ and $Au_2S(HS)_2^-$ species of gold have been taken from high-T experiments by Shenberger(1985) and Seward(1976) respectively while data for $Au(HS)^o$ at 25°C were obtained from Renders and Seward(1988). Stability data for gaseous and most of the solid phases were obtained from the databanks of CPDMRLDATA and CPDNBSDATA databanks. For other aqueous and solid species the data source was similar to that which was used for calculations on the solubility of platinum and has been summarized in table 3.

Gold Speciation in the System Au-Cl-S-H-O

The speciation of gold in aqueous solutions has been investigated by calculating a number of log f_{H2} - pH diagrams at fixed temperatures. The first series of these diagrams (Fig 13) has been calculated for solutions undersaturated in solid gold. The calculations have been carried out for solutions with total acivities of dissolved sulfur and chloride of 0.001 and 2 respectively. The second series of these diagrams (Fig 14) have been calculated with higher activities of dissolved gold in the system to depict solubility contours of gold. These calculations indicate that the solubility of gold as $AuCl_2^{-1}$ increases with decrease in pH and f_{H2} (increase in the redox

state) as anticipated from earlier studies. $AuCl_4^{-1}$ would become stable only at very low f_{H2} (high redox state) and/or highly acidic conditions. The solubility of gold as sulphide complexes changes in a complex manner increasing in a direction towards the "triple point" where aqueous H_2S, HS^- and SO_4^{-2} have equal activities. Fig 15 illustrates the effect of total dissolved chloride in the fluid on the solubility of gold. The solubility contours for 0.01 ppb of gold have been drawn at two different activities of total chloride (0.02 and 2.0) in the fluid. As expected, a drop in the activity of total chloride narrows down the field of predominance of $AuCl_2^-$ and the solubility contours move to lower f_{H2} (higher redox state) conditions.

The temperature dependence of gold speciation is depicted on a number of log f_{O2} - /T diagrams calculated for solution with the activities of total dissolved sulphur and chloride equal to 0.001 and 2 respectively. In these calculations, the pH of the system has been buffered by the Kmq assemblage at two different activities of total potassium (0.1 and 0.01) In the first series of such diagrams (Fig. 16) calculations have been made for solutions undersaturated with solid gold, whereas in Fig. 17 the system has been calculated for higher activity of dissolved gold. In the later case boundaries between solid gold and the aqueous species have been drawn for 0 .01 ppb of total dissolved gold. These calculations show that, under these conditions $AuCl_2^{-1}$ is the main chloro-complex of gold and $AuCl_4^{-1}$ could become stable only in highly acidic solutions (a_K =1) at a high redox state.

Solubility of Gold in Rock Buffered Fluid

The solubility of gold in a saline fluid with both pH as well as f_{O2} buffered by the mineral assemblages has been calculated for a fluid with activities of total dissolved chloride and sulfur equal to 2 and 0.001 respectively. The pH of the fluids has been buffered by the Kmq assemblage at three different activities of total dissolved potassium(1, 0.1 and and 0.01).

In fluids where the magnetite+hematite assemblage buffers the redox state (Fig 18), sulfide complexes of gold predominate over chloride complexes

though activity of $AuCl_2^-$ increases with temperature. At temperatures below100°C, $Au_2S(HS)_2^{-2}$ is the dominat sulphide complex while at higher temperatures, $Au(HS)_2^{-1}$ becomes dominant. Recent experimental studies on the speciation of gold in aqueous solution at 25°C (Renders and Seward,1987) have failed to record the presence of $Au_2S(HS)_2^{-2}$ as an aqueous complex of gold. Instead, $Au(HS)^o$ is believed to be the dominant aqueous complex at a pH more acidic than 3. Due to the lack of stability data for this complex at higher temperatures, it has not been possible to study the contribution of this particular complex to the solubility of gold at higher temperatures.

These calculations indicate that a saline (a_{Cl} = 2) fluid with pH buffered by the Kmq assemblage (Fig 18a) can dissolve upto about100 ppb of gold at 50°C . In the fluids which have their redox buffered by the $Mn_3O_4+Mn_2O_3$ assemblage, chloro-complexes of gold clearly predominate over the sulfide complexes (Fig 18). The solubility of gold increases from 0.01 ppb at 25°C to about 10 ppm at 250°C. The solubility of gold also increases with increase in the activity of dissolved chloride and decrease with increase in pH.

Solubility of Gold in Fluids Saturated with Atmospheric Oxygen

Fig. 19 represents solubility of gold in a saline fluid saturated with atmospheric oxygen. The pH of these fluids has been buffered by the Kmq assemblage. As expected, because of very high redox state, chloro-complexes of gold become the dominant aqueous complexes of gold. The solubility of gold increases with temperature e.g. a saline (a_{Cl}= 2), acidic (a_K=1) fluid can dissolve upto about 50 ppm of gold at 25°C while at 250°C, the same oxygen saturated fluid can dissolve 3 times more gold. The solubility of gold also increase with increase in the activity of chloride and potassium(equivalent to decrease in pH) in the fluid.

Possible mechanisms of deposition of gold

Calculations on the solubility of gold have clearly shown that saline, highly oxidized (saturated with atmospheric oxygen or buffered by the $Mn_3O_4+Mn_2O_3$ assmblage) fluids which are capable of transporting geologically

realistic concentrations of platinum are equally capable of transporting realistic amounts of dissolved gold. In order to investigate the effect of reacting of these fluids with reducing agent in depositing gold a number of calculations were carried out in which the gold-bearing saline and oxidized fluid reacts with graphite or magnetite at fixed temperature.

Fig. 21 show changes in the activity of aqueous species of gold as a fluid initially saturated with atmospheric oxygen starts reacting with graphite. . All these calculations show that reacion with very small amounts of reducing agent is able to precipitate the bulk of the dissolved gold.

Discussion and Conclusions

The study of gold solubility and its speciation in the system Au-Cl-S-H-O reveals the following important similarities in the solubility of gold and platinum in saline, acidic, oxidized fluids :

1. In saline (a_{Cl}=1 and 2) fluids gold forms both chloro- as well as sulfide complexes. The chloro species dominate in more acidic and more oxidized fluids whereas sulfide-complexes become dominant with increase in pH and drop in salinity and redox state.

2. The solubility of gold as chloro-complexes increases with increase in the redox state. In magnetite+hematite buffered fluids most of the gold is present as sulfide complexes and maximum solubility of gold is around 100 ppb at 50°C. In fluids where the redox state is buffered by the Mn_3O_4+Mn_2O_3 assemblage, sulfide species of gold become relatively unstable and maximum solubility of gold at 25°C is around 0.1 ppb increasing to 14 ppm at 250°C. In fluids saturated with atmospheric oxygen solubility of gold ranges between 20 and 160 ppm at 250°C depending upon the pH.

3. Thus, saline, acidic and oxygen- saturated fluids which are capable of transporting geologically significant amounts of platinum can also carry significant amounts of gold.

4. Reduction of oxidized fluids due to their reaction with magnetite and/or graphite bearing rocks which deposited most of the dissolved platinum is equally efficient in depositing gold from these fluids.

Application to the Genesis of PGE-Au Concentrations in the Unconformity Related Uranium Deposits

There is very little data available on the nature of PGE-Au mineralization in the unconformity- related uranium deposits except at the Coronation Hill U/Au mine (Needham, 1987). In this deposit the main rock types are: altered felsic volcanics, tuffaceous sediments, sandstone, felsic porphyry (Coronation sandstone), carbonaceous shales(Koolpin Formation) and minor altered mafic igneous rocks(Zamu dolerite). The bulk of the PGE-Au mineralization is hosted by the altered volcanics and the Coronation sandstones. The host rocks are hematitized, sericitised and silicified with some minor pyrite, chlorite and vein quartz. The gold is finely disseminated and a reserve of 800,000 t of ores at an average grade of 5g/t has been estimated. Gold bearing samples (>1g/t Au) contain an average of 0.62g/t of Pt and 1.33g/t of Pd.

According to Needham (1987) gold veins cut across the pitchblende mineralization and hence are later than the uranium mineralization. The PGE mineralization, which shows close spatial association with the gold mineralization in all probability formed at the same time.

Calculations described in the previous sections have shown that saline(a_{Cl} =1), Kmq and/or Kcq(potash feldspar+kaolinite+quartz) buffered fluids (a_K=0.01) and saturated with atmospheric oxygen are capable of dissolving geologically realistic amounts of platinum (upto 60 ppm at 25°C) and gold (160 ppb at 25°C). It was also shown that reaction of such fluids with low redox state buffers (due to reaction with carbonaceous material, graphite, Fe^{+2} minerals etc.) causes an appreciable drop in their solubility. Hence, in order to generate economic concentrations of PGE-Au in the unconformity-related deposits through these fluids, it is essential that these fluids maintain their high redox state while flowing through the aquifer(sandstone and/or volcanics). It has been mentioned earlier that in many unconformity-related uranium deposits sedimentary rocks (sandstones) overlying the unconformity surface show mineralogical and chemical characteristics indicating their deposition and/or diagenesis under high redox conditions (hematitic red beds). Ore fluids

saturated with atmospheric oxygen flowing through such a rock would maintain their high redox state because these fluids would have negligibly small concentration of Fe^{+2} and the rocks would be rich in Fe^{+3} phases.More realistically, the oxygen- saturated fluids while flowing through such a rock would first oxidizeany residual Fe^{+2} phases, allowing subsequent batches of ore fluids to retain their high redox state. The oxidizing ore fluids would move the oxidation-reduction interface deeper and deeper into the aquifer, leaching and redepositing platinum and gold mineralization. From this point of view the whole sytem would be very identical to that which is generally accepted for the roll-type uranium deposits (e.g. DeVoto, 1978). The capacity of the oxygen-saturated ore fluids to maintain their high redox state after infiltrating into the aquifer will depend on the fluid/rock ratio and the fluid-flow rates. In order to estimate the magnitude of the possible fluid/rock ratios, a number of mass-balance calculations were performed in which a fixed quantity of rock of known composition was titrated against an oxygen-saturated fluid at a given temperature. In these calculations a rock containing (in wt%) 94% quartz, 3% kaolinite, 1.5% potash-feldspar, 1% sericite and 1% magnetite was titrated at 100°C against an oxygen-saturated fluid containing (in moles/Kg) 55.52 moles of water, $0.2x10^{-3}$ moles of dissolved oxygen, 1mole of dissolved chloride, 0.02 moles of potassium and 0.98 moles of sodium. These calculations show that a fluid/rock ratio of about 6 is sufficient to oxidize all the Fe^{+2} in $1m^3$ of the rock to Fe^{+3} phases (hematite). An alternative way of estimating the amount of the fluid/rock interaction in the abovementioned conditions could be based on the estimation of time required to oxidize a fixed amount of Fe^{+2} in an aquifer calculated based on a geologically realistic fluid-flux rate. Such calculations show that in a basin with 300 Km^3 of sandstone aquifer, containing 0.1wt% of Fe^{+2} mineral phases (magnetite), it would take upto about 10 my. to oxidize total Fe^{+2}. These calculations are based on an assumed fluid-flux rate of about $0.01m^3/m^2.day$. According to Habermehl (1980), the main aquifers in the Great Artesian Basin of Australia belonging to the lower Cretaceous-Jurassic sequence have

hydraulic conductivities in the range of 0.1 to 10 $m^3/m^2.day$ (hydraulic gradients for the aquifers range between 1:2000 and 1:1800). Given the extended tectonically stable postdepositional history of the Kombolgie basin it seems quite realistic to suppose that oxygen-saturated saline surface waters could maintain some free oxygen while flowing through the oxidized aquifer, thereby leaching PGE and gold (and probably uranium) from any oxidized source rock. Redeposition will occur at any oxidation/reduction interface containing Fe^{2+} minerals, which in the case of the unconformity-related deposits is provided by post-Kombolgie fault breccias exposing fresh (unoxidized) basement rocks (Wilde and Wall, 1987). Fluids of moderate to high salinity could be either generated by subsurface evaporite dissolution or by surface evaporation. Shallow saline groundwaters are common in arid regions, and are typically moderately to highly acid (e.g Mann, 1983; Teller et al, 1982).

The presence of a source rock for PGE and gold is another crucial requirement, which needs further study. The most likely possibilities for deposits like Coronation Hill are:

1. High-energy clastic sediments and conglomerates, which could contain the precious metals as placer concentrations

2. Volcanics, particularly the felsic volcanics that are commonly intersected and deeply weathered at the unconformity in the South Alligator River valley.

3. Mafic igneous rocks such as dolerites (Zamu dolerite or Oenpelli dolerites), or minor basalts within the Kombolgie formation.

References

1. Ayres, D.E and Eadington, P.J., 1975, Uranium mineralization in the South Alligator River valley: Mineral. Deposita, v.10, p. 27-41.
2. Bowles, J.F.W., 1986, The development of platinum-group minerals in laterites: Econ. Geol, v.81, p. 1278-1285.
3. Brookins, D.G., 1987, Platinoid element Eh-pH diagram(25oC, 1bar) in the system M-O-H-S with geochemical applications: Chem. Geol, v.64, p. 17-24.
4. Cobble, J.W., Murray, Jr., R.C., Turner, P.J and Chen, K., 1982, High temperature thermodynamic data for species in aqueous solution: Nat.Tech.Inform. Service Rept. EPRI-NP- 2400, p. 1-197.
5. Criss, C.M., and Cobble, J.W., 1964, The thermodynamic properties of high-temperature aqueous solutions: Jour. Am. Chem. Soc., v86, p 5385-5393
6. Dahlkamp, F.J., 1978, Gelogical appraisal of the Key Lake U- Ni deposits, Northern Saskatchewan: Econ. Geol, v.73, p. 1430-1449.
7. DeVoto, R.H., 1978, Uranium in phanerozoic sandstone and volcanic rocks. Short course in Uranium deposits: Their mineralogy and origin., MAC short course handbook v3., p. 293-305.
8. Drummond, S.E., 1981, Boiling and mixing of hydrothermal fluids: Chemical effects on mineral precipitation: Unpub. Ph.D thesis, The Pennsylvania State Univ., 380 p.
9. Faramazyan, A.S., Kalinin, S.K and Terekhovich S.L, 1975, Geochemistry ofplatinum group elements in the ores of copper-molybdenum deposits of Armenia: Dokl. Akad. Nauk SSSR, v.190, p. 220- 221.
10. Fuchs, A.W and Rose, A.W, 1974, The geochemical behaviour of platinum and palladium in the weathering cycle in the Stillwater Complex, Montana: Econ. Geol, v.69, p.332-346.

11. Giggenbach, W.F, 1980, Geothermal-gas equilibria: Geochimi. et Cosmochimi. Acta, v.44, p. 2021-2032.

12. Goldberg, R.N and Hepler, L.G, 1968, Thermochemistry and oxidation potential of the platinum group metals and their compounds: Chem. Rev, v.68, p.229-252.

13. Hakli, T.A., Hanninen, E., Vuorelainen, Y and Papunen, H., 1976, Platinum-group minerals in the Hitura nickel deposit, Finland: Econ. Geol., v.71, p. 1206-1213.

14. Habermehl, M.A., 1980, The Great artesian basin, Australia: BMR Jour. Austraian Geol. Geophysics, 5, p.9-38.

15. Hegge, M.R., Mosher, D.V., Eupene, G.S and Anthony, P.J., 1980, Geological seting of the East Alligator uranium deposits and prospects: Proceedings of the International Uranium symposium, IAEA, p. 259-272.

16. Heinrich, C.A., 1987, The CSIRO-SGTE-THERMODATA package for thermodynamic computations at BMR: Records BMR, Geology and Geophysics, 1987/42, p. 44.

17. Helgeson, H. C., 1969, Thermodynamics of hydrothermal systems at elevated temperatures and pressure: Am. J. Sci., v. 267, p. 729-804.

18. Henley, R.W., Truesdell, A.H., Barton,Jr., P.B, 1984, Fluid-mineral equilibria in hydrothermal systems: Reviews in Economic Geology, v.1, SEG, 267 p.

19. Hoeve, J and Sibbald, T.I.I., 1978a, On the genesis of Rabbit Lake and other unconformity-type uranium deposits in Northern Saskatchewan, Canada: Econ. Geol., v.73, p.1450-1473.

20. Hoeve, J and Sibbald, T. I.I., 1978b, Mineralogy and geological setting of the unconformity-type uranium deposits in Northern Saskatchewan., Short course in Uranium deposits: Their mineralogy and origin., MAC short course handbook v3, p.457-474.

21. Kucha, H., 1982, Platinum-group metals in the Zechstein copper deposits, Poland: Econ. Geol., v.77, p. 1587-1591.

22. Maas, R., McCulloch, M.T., Page, R.W., and Campbell, I. H., 1986, Sm-Nd isotopic systematics of uranium deposits (abs.): Terra Cognita, v. 6, p. 225.

23. Mann, A.W., 1984, Mobility of gold and silver in lateritic weathering profiles: some observations from W.Austraia: Econ. Geol., v.79, p. 38-49.

24. Mihalik, P., Jacobson, J.B.E and Hiemstra, S.A., 1974, Platinum-group minerals from a hydrothermal enviornment: Econ. Geol., v.69, p. 257-262.

25. Mountain, B.W. and Wood, S.A., 1987, Solubility and transport of PGE in hydrothermal solutions to 300°C: Thermodynamic calcultions: Abstr., Geo-Platinum 87 symposium, The Open University, Milton Keynes, U.K

26. Murray, Jr., R.C., and Cubicciotti, D., 1983, Thermodynamics of aqueous sulfur species at 300°C and potential-pH diagrams: J. Electrochem.Soc., v. 130, p. 866-869.

27. Naumov, G.B., Ryzhenko, B. N., Khadakovski, Y.L, 1971, Handbook of thermodynamic data. English Translation (ed. H. Barnes and V.Speltz) USGS-Report WRD-74-001 (1974)

28. Needham, R.S., 1987, A review of mineralization in the South Alligator conservation zone: Records, BMR, Geology and Geophysics., 1987/52, pp.13.

29. Needham, R.S. and Stuart-Smith, P.G., 1987, Coronation Hill U-Au mine, South Alligator valley, Northern Territory: an epigenetic sandstone-type deposit hosted by debris-flow conglomerate: BMR Journal of Australian Geology and Geophysics., v.10, p. 121-131.

30. Ottemann, J. and Augustithis, S.S., 1967, Geochemistry and origin of "platinum-nuggets" in lateritic covers from ultrabasic rocks and birbirites of W.Ethiopia: Mineral. Deposita., v.1, p. 269-277.

31. Pagel, M., Poty, B. and Sheppard, S.M.F., 1980, Contribution to some Saskatchewan uranium deposits mainly from fluid inclusion data: Proceedings of International Uranium symposium on the Pine Creek geosyncline., IAEA., p. 639- 654.

32. Peyrel, W., 1982, The influence of the Driekop dunite pipe on the platinum-group mineralogy of the UG-2 chromitite in its vicinity: Econ. Geol., v.77, p. 1432-1438.

33. Pispanen, M. and Tarkian, M., 1984, Cu-Ni-PGE mineralization at Rometolvas, Koillismaa layered igneous complex, Finland: Mineral. Deposita., v.19, p. 105-111.

34. Ramaekers, B., and Dunn, C.E, 1977, Geology and geochemistry of the eastern margin of the Athabasca Basin: In: Uranium in Saskatchewan(Dunn, C.E., ed.), Sask. Geol. Soc. Spec. Publ., 3, 297-322.

35. Renders, P.J., Sewards, T.M, 1988, The stability of Hydrosulphide and sulphide complexes of Au(I) at 20°C. Paper submitted to Geochim. Cosmochim. Acta

36. Ruaya, J.R., 1986, The satbility of metal chloride complexes in hydrothermal solutions: Unpubl. Ph.D thesis., Victoria University of Wellington.

37. Tarkian, M. and Stumpfl, E.F., 1975, Platinum mineralogy of the Dreikop mine, South Africa: Mineral. Deposita., v.10, p. 71-85.

38. Teller, J.T., Bowler, J.M. and Macumber, P.G., 1982, Modern sedimetation and hydrology in Lake Tyrrell, Victoria: Journal of the Geological Society of Australia., v.29, p. 159-175.

39. Trocki, L.K, Curtis, D., Gancarz, A.J. and Banar, J.C., 1984, Ages of major uranium mineralization and lead loss in the Key Lake uranium deposit, Northern Saskatchewan, Canada: Econ. Geol., v.79, p. 1378-1386.

40. Turnbull, A. and Wadsley, M.W., 1986, The CSIRO-SGTE THREMODATA system. Introduction: Databank index; FILER; ESTIMA; REACT; CHEMIX; VAPOUR; ENERGY; 9 vols: CSIRO Div. Mineral Chemistry. Port Melbourne.

41. Wagman, D.D., Evans, W.H., Parker, V.B., Schumm, R.H., Halow, I., Bailey, S.M., Churney, K.L. and Nutall, R.L., 1982, The NBS tables of chemical thermodynamic properies: Journal of Physical and Chemical Reference data., v.11, p. 392.

42. Westland, A.D., 1981, Inorganic chemistry of the platinum- group elements: Canadian I.M.M., special v.23, p. 7-18.

43. Wilde, A.R and Wall, V.J., 1987 Geology of the Nabarlek Uranium deposit: Econ. Geol., v. 82, p. 1152-1168.

44. Wray, E.M., Ayres, D.E. and Ibrahim, H., 1986, Geology of the Midwest uranium deposit, Northern Saskatchewan: Canadian I.M.M., special v.32, p. 54-66.

45. Yang, Min-chin., Ni Chi-tsung. and Tai Feng-fu, 1974, Geochemistry of precious metals in skarns and hydrothermal copper deposits from a certain district in China: Geochimica., v.9, p. 167-180. (in Chinease with Engl. summary).

46. Ypma, P.J.M. and Fuzikawa, K., 1980, Fluid inclusion and oxygen isotope studies of the Nabarlek and Jabiluka uranium deposits, Northern Territory, Australia: Proceedings of International uranium symposium on the Pine Creek geosyncline: IAEA., p. 375-395.

47. Yushko-Zakharova, O.Ye., Ivanov, V.V., Razina, L.S. and Chernyayev, L.A., 967, Geochemistry of platinum metals: Geochemistry International.,v.4, p. 1106-1107.

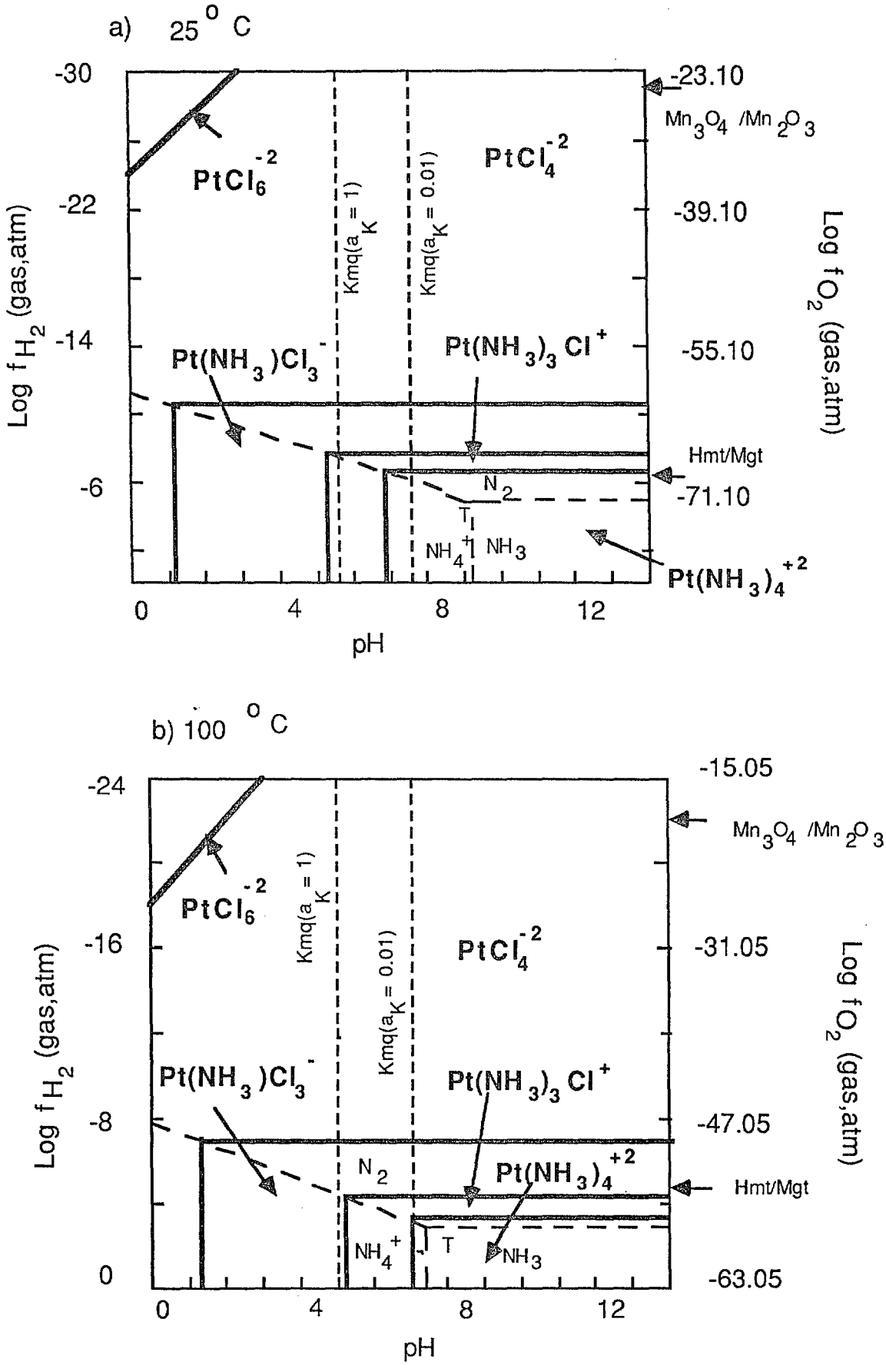
a) 25 °C
-30
-22
-14
-6
Log f H2 (gas,atm)
PtCl6 -2
PtCl4 -2
Kmq(aK = 1)
Kmq(aK = 0.01)
Pt(NH3)Cl3 -
Pt(NH3)3 Cl +
N2
T
NH4 +
NH3
Pt(NH3)4 +2
0
4
8
12
pH
-23.10
Mn3O4 /Mn2O3
-39.10
-55.10
Hmt/Mgt
-71.10
Log fO2 (gas,atm)
b) 100 °C
-24
-16
-8
0
-15.05
-31.05
-47.05
-63.05
T

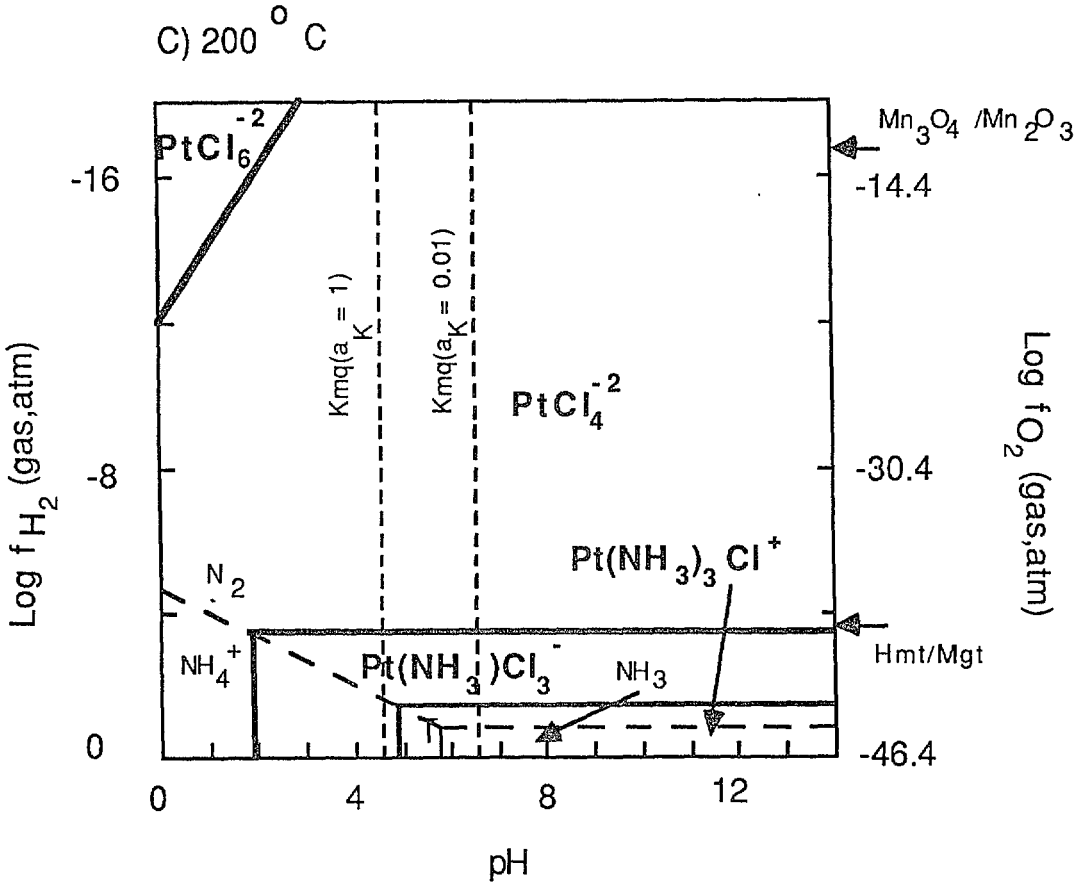

Fig. 1. Log f_{H2} - pH diagrams showing the stability fields of aqueous species of platinum. Also shown along the right ordinate axis are the corresponding Log f_{O2} values. Calculations have been made for $a_{Cl^-} = 2$, $a_{dissolved\ N} = 1$. Dashed lines denote the stability fields of aqueous species of nitrogen, while solid lines denote the stability fields of aqueous species of platinum. The system is undersaturated with solid platinum phases. Dashed vertical lines represent Kmq (potash feldspar+muscovite+quartz) buffer assemblage at two different activities of dissolved potassium (1 and 0 .01). Arrows on the right ordinate axis indicate positions of Hmt/Mgt (hematite+magnetite) and Mn_3O_4+Mn_2O_3 redox buffer assemblages. Triple point marked T indicates the point of equal activity of aqueous N_2, NH_3 and NH_4^+. a - 25°C, b- 100°C, c - 200°C.

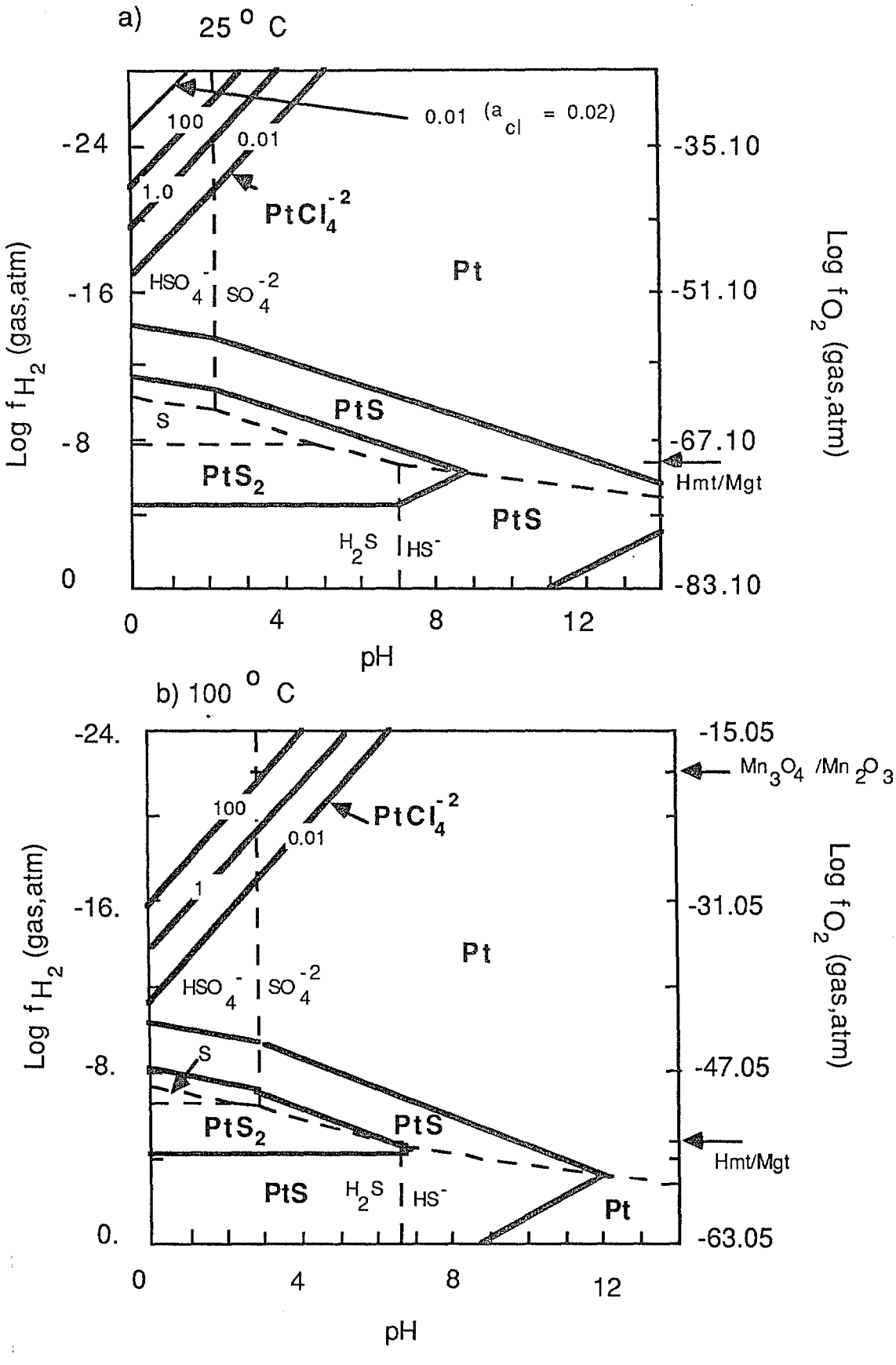
a) 25 °C
100
0.01
1.0
0.01 (a cl = 0.02)
PtCl4-2
Pt
HSO4- SO4-2
PtS
S
PtS2
PtS
H2S HS-
-24
-16
-8
0
-35.10
-51.10
-67.10
-83.10
Hmt/Mgt
Log fH2 (gas,atm)
Log fO2 (gas,atm)
0
4
8
12
pH
b) 100 °C
-24.
-16.
-8.
0.
-15.05
-31.05
-47.05
-63.05
Mn3O4 /Mn2O3
Hmt/Mgt
100
1
0.01
PtCl4-2
Pt
HSO4- SO4-2
S
PtS2
PtS
PtS
H2S HS-
Pt
Log fH2 (gas,atm)
Log fO2 (gas,atm)
0
4
8
12
pH

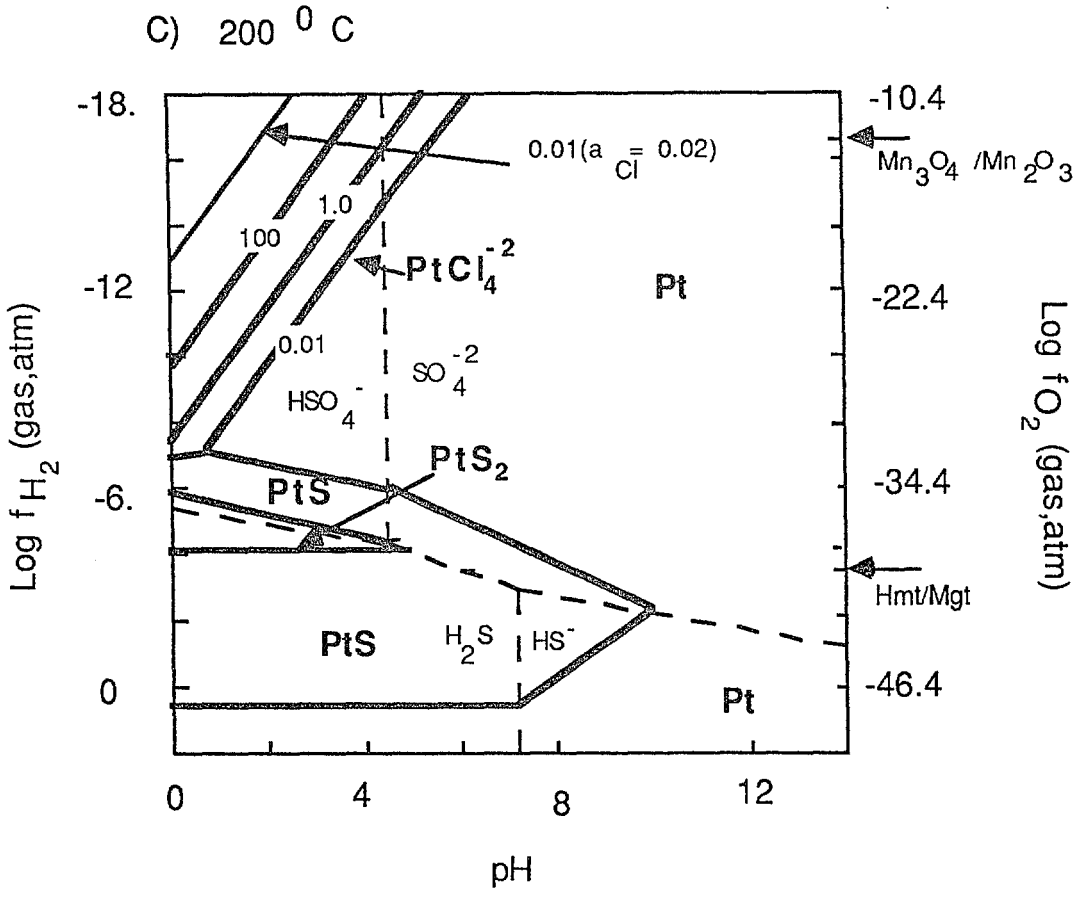

Fig. 2. Log f_{H_2} - pH diagrams showing the stability fields of solid phases of platinum along with the solubility contours of dissolved platinum (as aqueous $PtCl_4^{-2)}$. Also shown along the right ordinate axis are the corresponding Log f_{O2} values. Calculations have been made for $a_{Cl^-} = 2$, a $_{\text{dissolved N}} = 1$ and $a_{\text{dissoved S}} = 0.001$. Dashed lines denote the stability fields of aqueous species of sulfur, while solid lines denote the stability fields of solid phases of platinum and the solubility contours in ppb of platinum. Arrows on the right ordinate axis indicate positions of Hmt/Mgt (hematite+magnetite) and Mn_3O_4+Mn_2O_3 redox buffer assemblages. In order to demonstrate the effect of changes in the activity of chloride on the solubility of platinum, solubility contour of 0.01 ppb of dissolved platinum at $a_{Cl} = 0.02$ has been shown as thin line. a- 25°C, b - 100°C, c - 200°C.

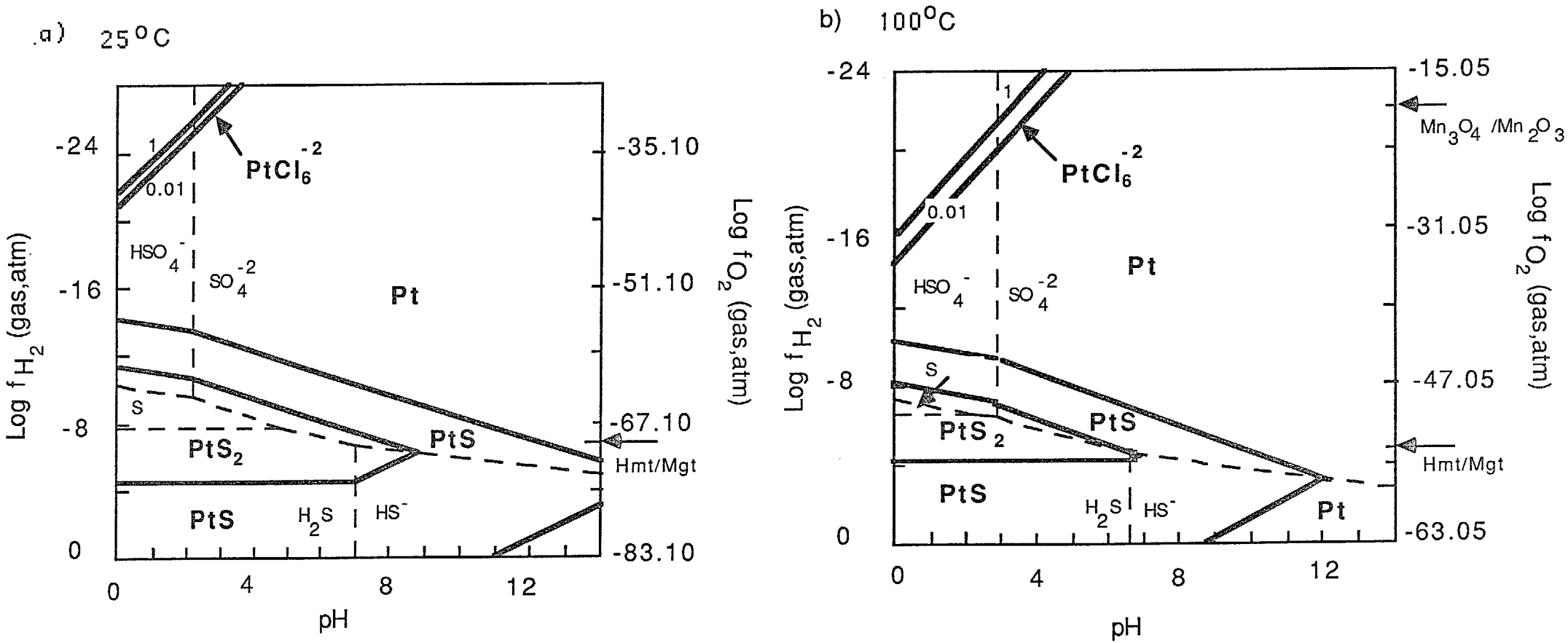

Fig. 3. Log f_{H_2} - pH diagrams showing the stability fields of solid phases of platinum along with the solubility contours of dissolved platinum (as aqueous $PtCl_6^{-2}$). Also shown along the right ordinate axis are the corresponding Log f_{O_2} values. Calculations have been made for $a_{Cl^-} = 2$, $a_{\text{dissolved N}} = 1$ and $a_{\text{dissoved S}} = 0.001$. Dashed lines denote the stability fields of aqueous species of sulfur, while solid lines denote the stability fields of solid phases of platinum and the solubility contours in ppb of platinum. Arrows on the right ordinate axis indicate positions of Hmt/Mgt (hematite+magnetite) and Mn_3O_4+Mn_2O_3 redox buffer assemblages. a- 25°C, b - 100°C.

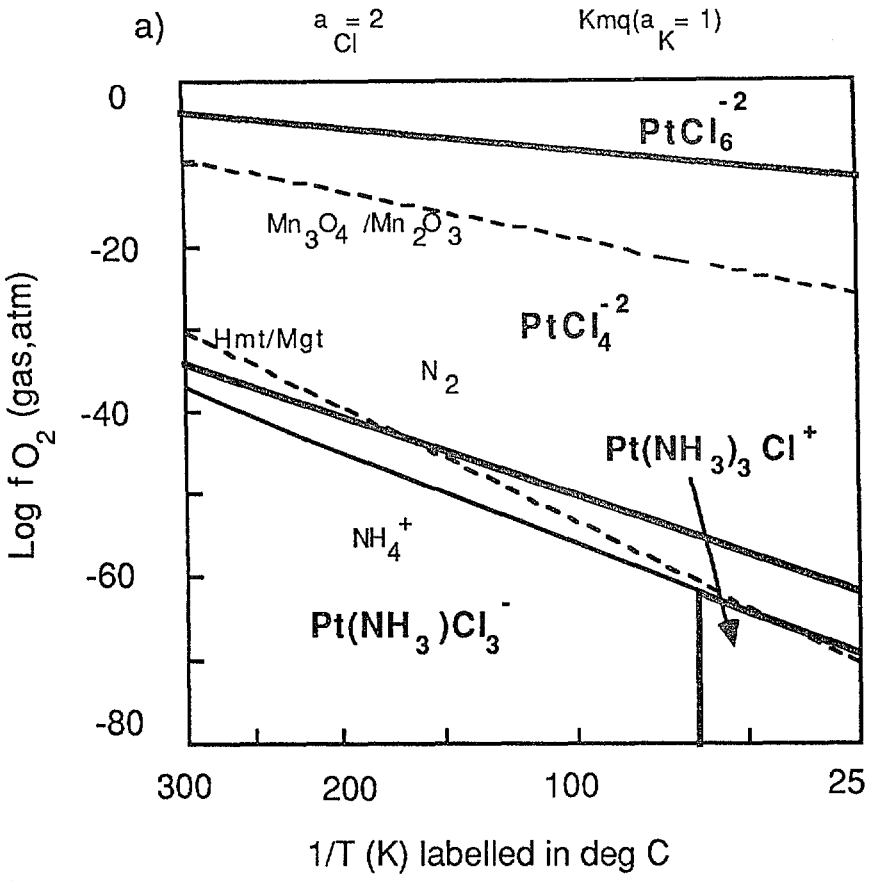
a)
$a_{Cl} = 2$
Kmq(a_K = 1)
0
-20
-40
-60
-80
Log fO_2 (gas,atm)
$PtCl_6^{-2}$
Mn_3O_4 /Mn_2O_3
$PtCl_4^{-2}$
Hmt/Mgt
N_2
$Pt(NH_3)_3Cl^+$
NH_4^+
$Pt(NH_3)Cl_3^-$
300
200
100
25
1/T (K) labelled in deg C

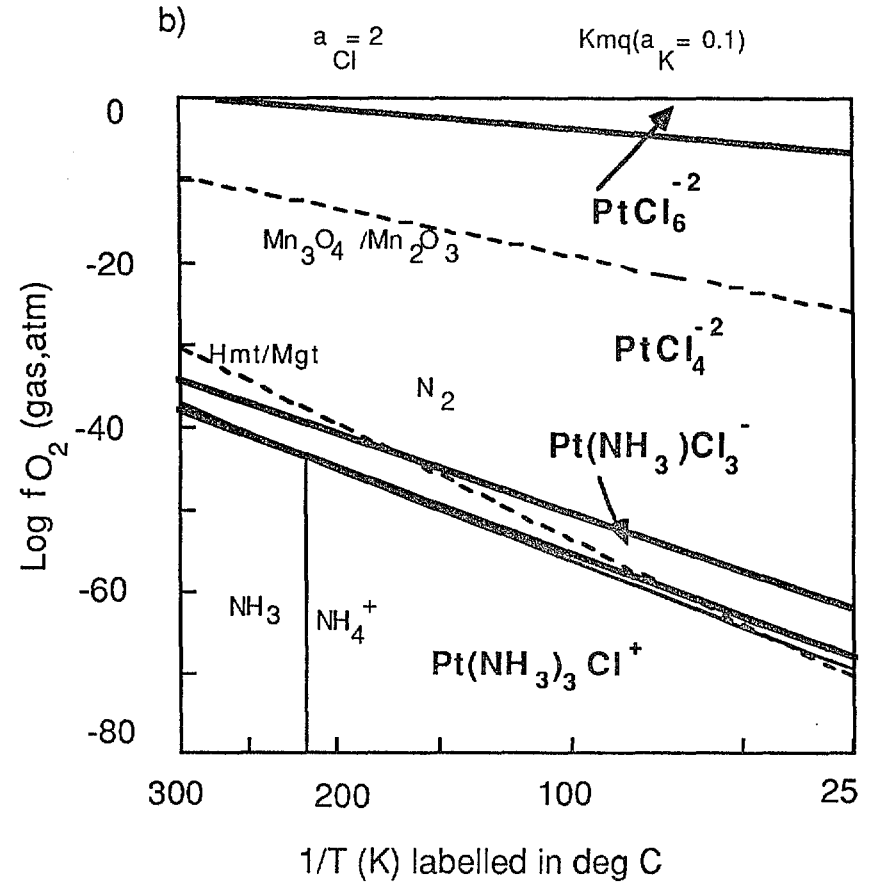
b)
$a_{Cl} = 2$
Kmq(a_K = 0.1)
0
-20
-40
-60
-80
Log fO_2 (gas,atm)
$PtCl_6^{-2}$
Mn_3O_4 /Mn_2O_3
$PtCl_4^{-2}$
Hmt/Mgt
N_2
$Pt(NH_3)Cl_3^-$
NH_3
NH_4^+
$Pt(NH_3)_3Cl^+$
300
200
100
25
1/T (K) labelled in deg C

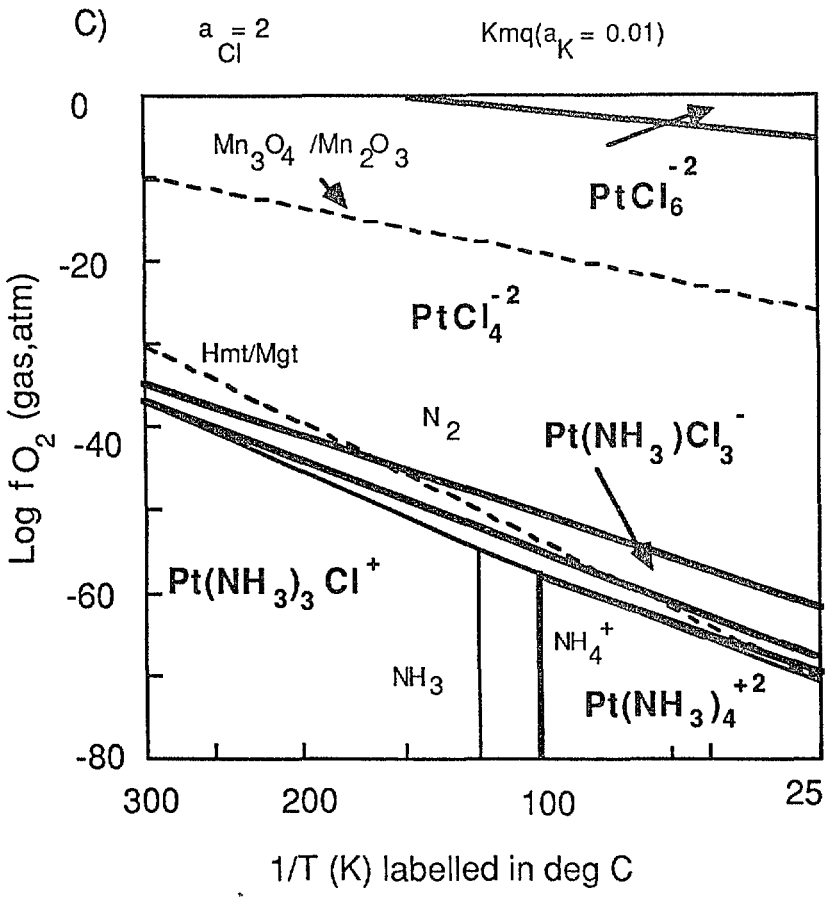

Fig. 4. Log f_{O_2} - 1/T diagrams showing the stability fields of aqueous species of platinum in a fluid buffered by the Kmq assemblage. Calculations have been done for $a_{Cl^-} = 2$ and $a_{\text{total dissolved N}} = 1$. Dashed lines denote boundaries between the aqueous speccies of nitrogen. Solid lines denote the stability fields of aqueous species of platinum. The system is undersaturated with soild platinum phases. Dashed lines represent $Mn_3O_4 + Mn_2O_3$ and magnetite+hematite buffer lines. a - $a_{K^+} = 1$, b - $a_{K^+} = 0.1$ c - $a_{K^+} = 0.01$.

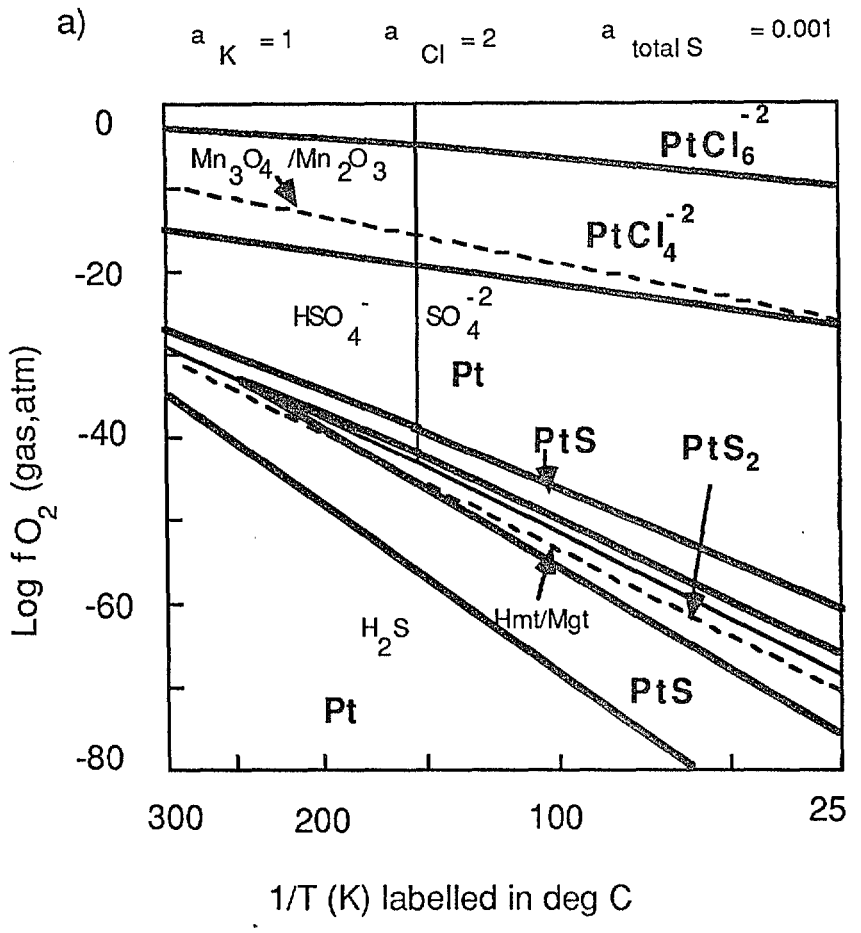
a)
a K = 1
a Cl = 2
a total S = 0.001
0
-20
-40
-60
-80
Log f O2 (gas,atm)
Mn3O4 /Mn2O3
PtCl6 -2
PtCl4 -2
HSO4 -
SO4 -2
Pt
PtS
PtS2
Hmt/Mgt
H2S
Pt
PtS
300
200
100
25
1/T (K) labelled in deg C

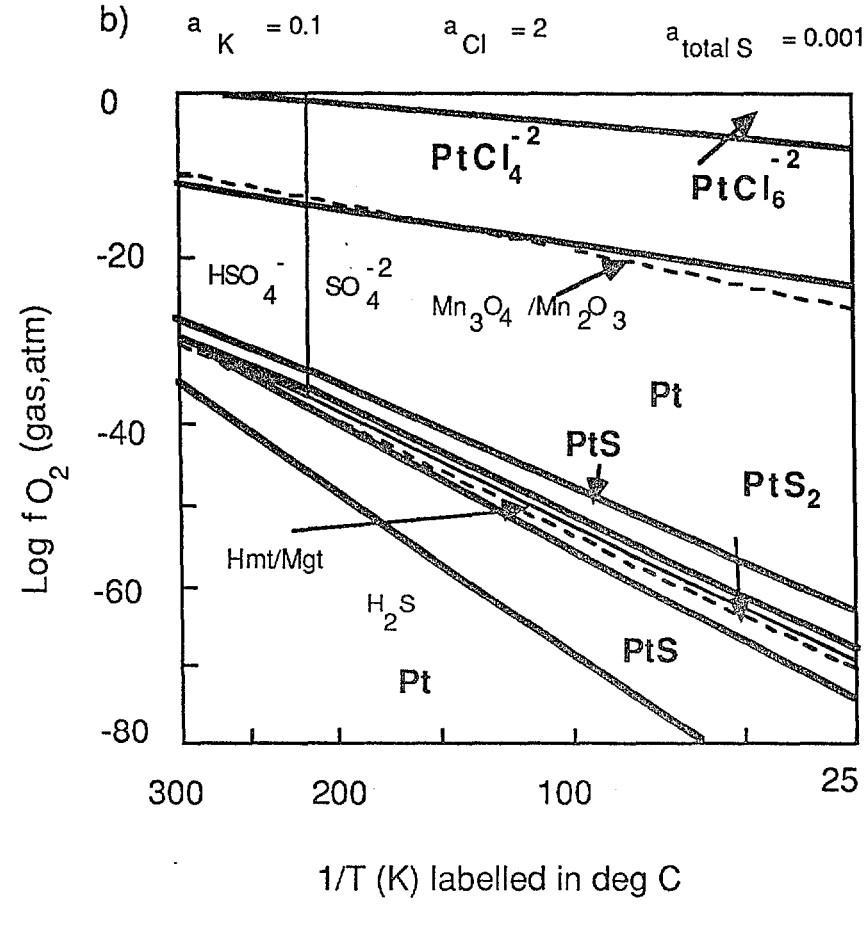
b)
a K = 0.1
a Cl = 2
a total S = 0.001
0
-20
-40
-60
-80
Log f O2 (gas,atm)
PtCl4 -2
PtCl6 -2
HSO4 -
SO4 -2
Mn3O4 /Mn2O3
Pt
PtS
PtS2
Hmt/Mgt
H2S
Pt
PtS
300
200
100
25
1/T (K) labelled in deg C

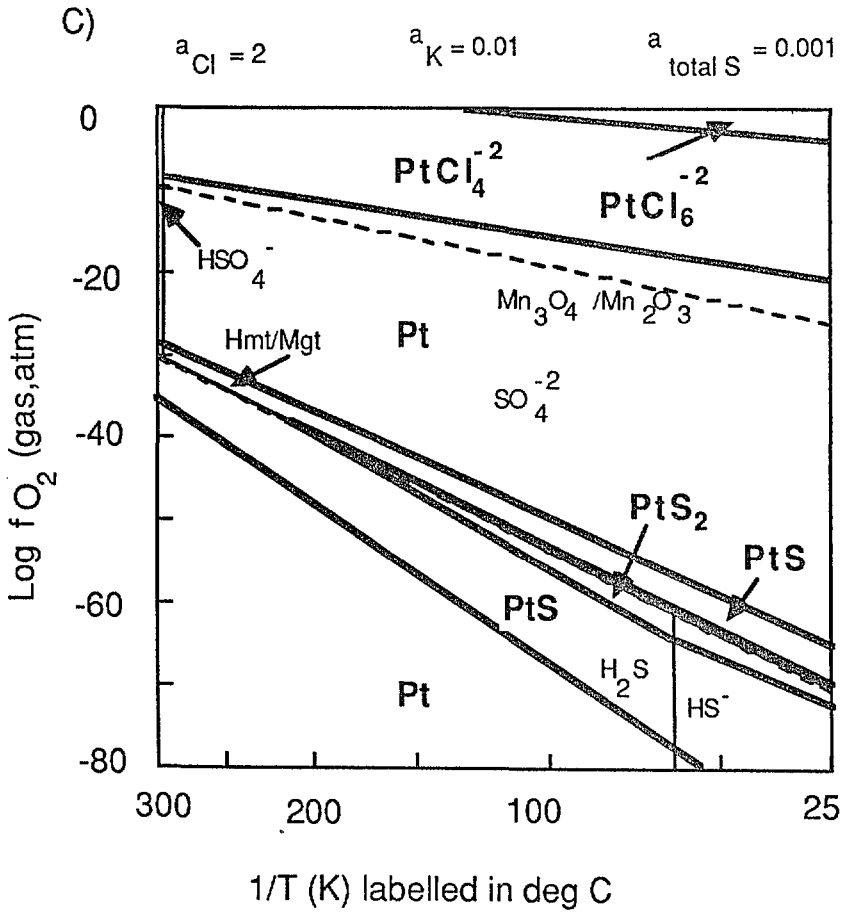

Fig. 5. Log f_{O_2} - 1/T diagrams showing the stability fields of aqueous species of platinum in a fluid buffered by the Kmq assemblage. Calculations have been done for $a_{Cl^-} = 2$ and $a_{\text{total dissolved S}} = 0.001$. Dashed lines denote boundaries between the aqueousspeceies of sulfur. Solid lines denote the stability fields of aqueous and solid phases of platinum. Boundaries between the solid phases platinum and the aqueous species have been drawn for 0.01 ppb of total dissolved platinum. Dashed lines represent $Mn_3O_4 + Mn_2O_3$ and magnetite+hematite buffer lines. a - $a_{K^+} = 1$, b - $a_{K^+} = 0.1$, c - $a_{K^+} = 0.01$.

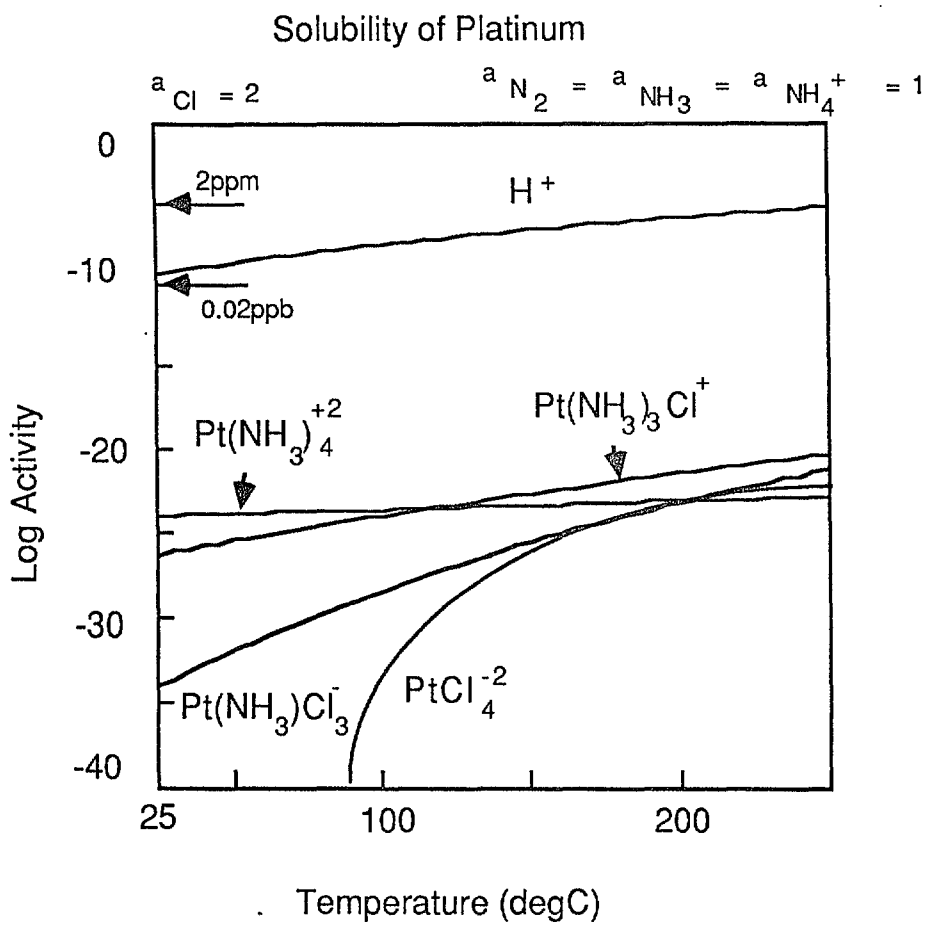

Fig. 6. Diagram showing variation in the solubility of platinum(as log activity of aqueous species) with temperature in a fluid buffered by the aqueous species of nitrogen. $a_{N2} = a_{NH3} = a_{NH4^+}$ (aq) = 1. $a_{Cl^-} = 2$. Numbers near the left ordinate axis represent approximate metal concentration.

a)

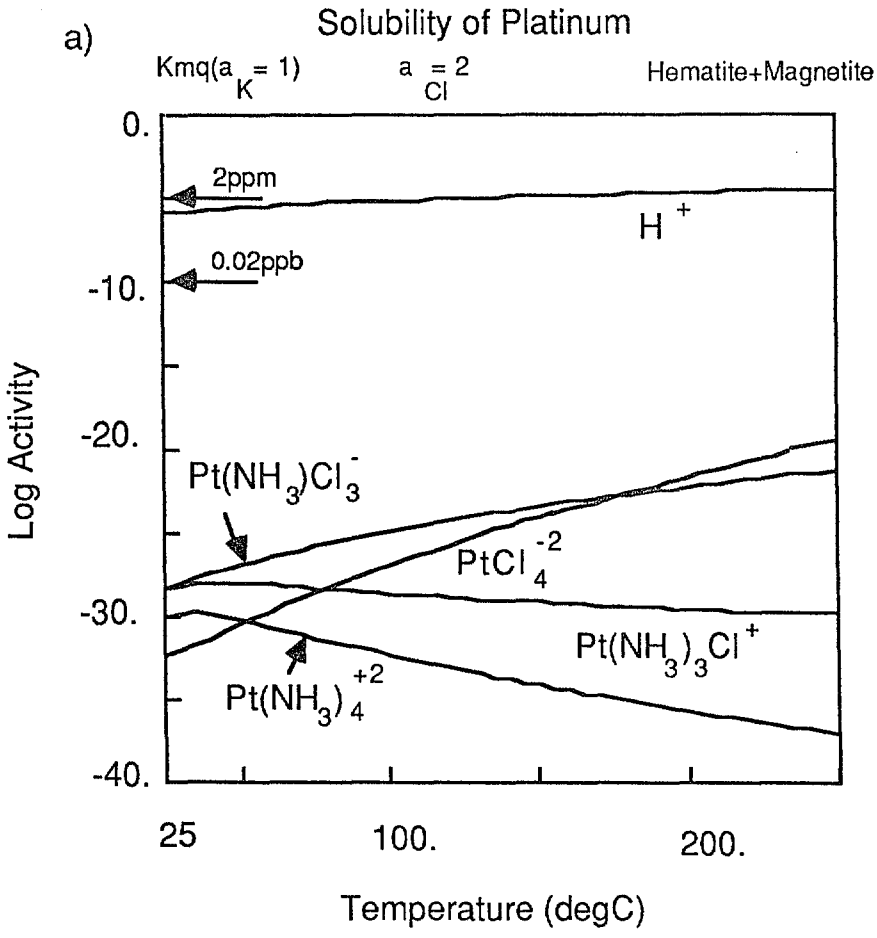
Solubility of Platinum
Kmq(a K = 1)
a Cl = 2
Hematite+Magnetite
0.
-10.
-20.
-30.
-40.
2ppm
0.02ppb
H +
Pt(NH3)Cl3 -
PtCl4 -2
Pt(NH3)3Cl +
Pt(NH3)4 +2
Log Activity
25
100.
200.
Temperature (degC)

b)

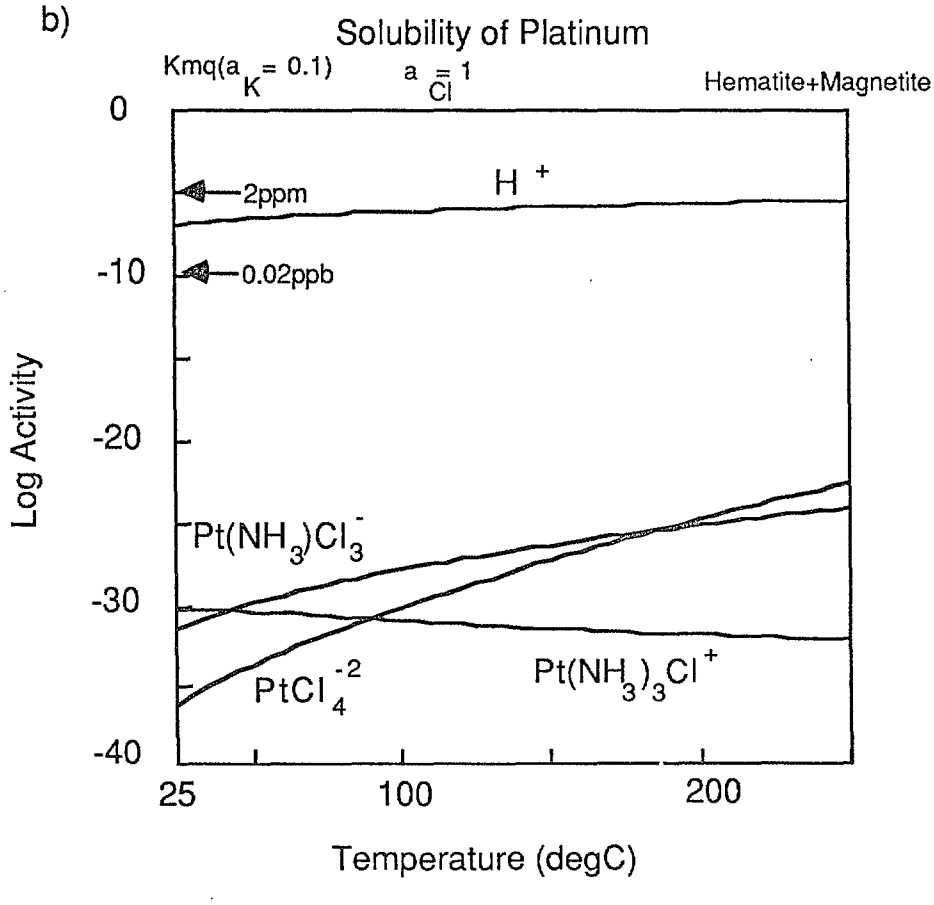
Solubility of Platinum
Kmq(a K = 0.1)
a Cl = 1
Hematite+Magnetite
0
-10
-20
-30
-40
2ppm
0.02ppb
H +
Pt(NH3)Cl3 -
PtCl4 -2
Pt(NH3)3Cl +
Log Activity
25
100
200
Temperature (degC)

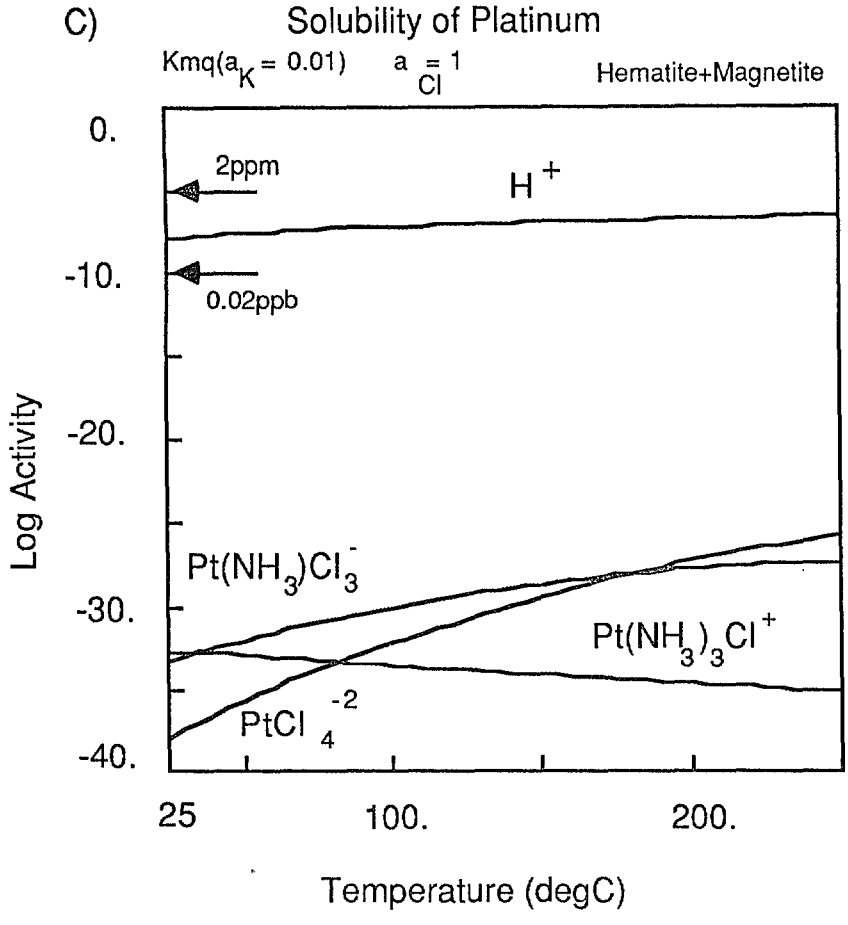

Fig. 7. Diagram showing variation in the solubility of platinum (as log activity of aqueous species) with temperature in a fluid buffered by the Kmq and magnetite+hematite assemblages. Numbers near the left ordinate axis represent approximate metal concentration. $a_{\text{total dissolved N}}$ =1. a - a_{Cl^-} = 2, a_{K^+} = 1, b - a_{Cl^-} = 1, a_{K^+} =0.1, c - a_{Cl^-} = 1, a_{K^+} = 0.01.

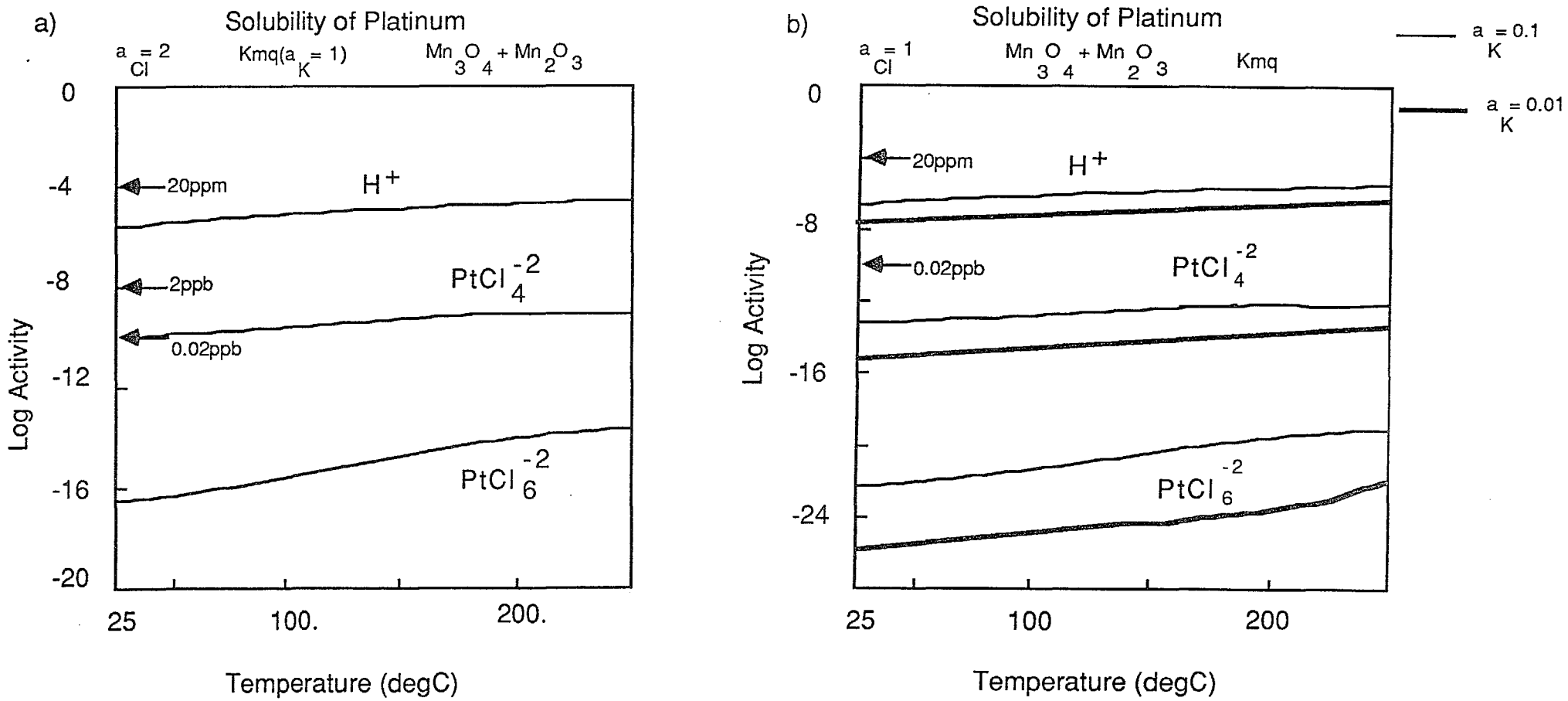

Fig. 8. Diagram showing variation in the solubility of platinum (as log activity of aqueous species) with temperature in a fluid buffered by the Kmq and Mn_3O_4+Mn_2O_3 assemblages. Numbers near the left ordinate axis represent approximate metal concentration. $a_{\text{total dissolved N}} = 1$, a - $a_{Cl^-} = 2$, $a_{K^+} = 1$, b - $a_{Cl^-} = 1$, $a_{K^+} = 0.1$ and 0.01.

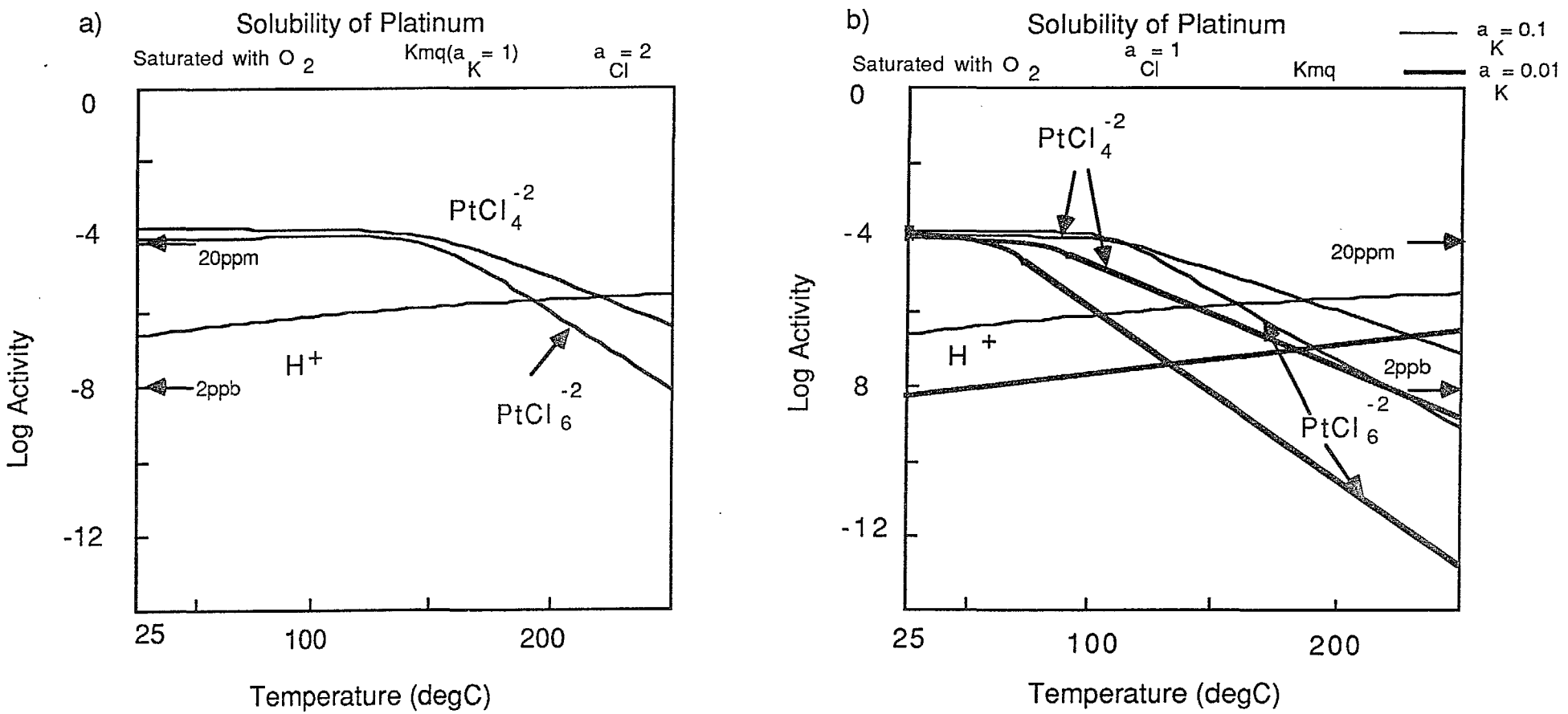

Fig. 9. Diagram showing variation in the solubility of platinum (as log activity of aqueous species) with temperature in a fluid saturated with atmospheric oxygen and buffered by the Kmq assemblage. Numbers near the left and right ordinate axes represent approximate metal concentration. $a_{total\ dissolved\ N}$ = 1. a - a_{Cl^-} = 2, a_{K^+} = 1, b - a_{Cl^-} = 1, a_{K^+} = 0.1 and 0.01.

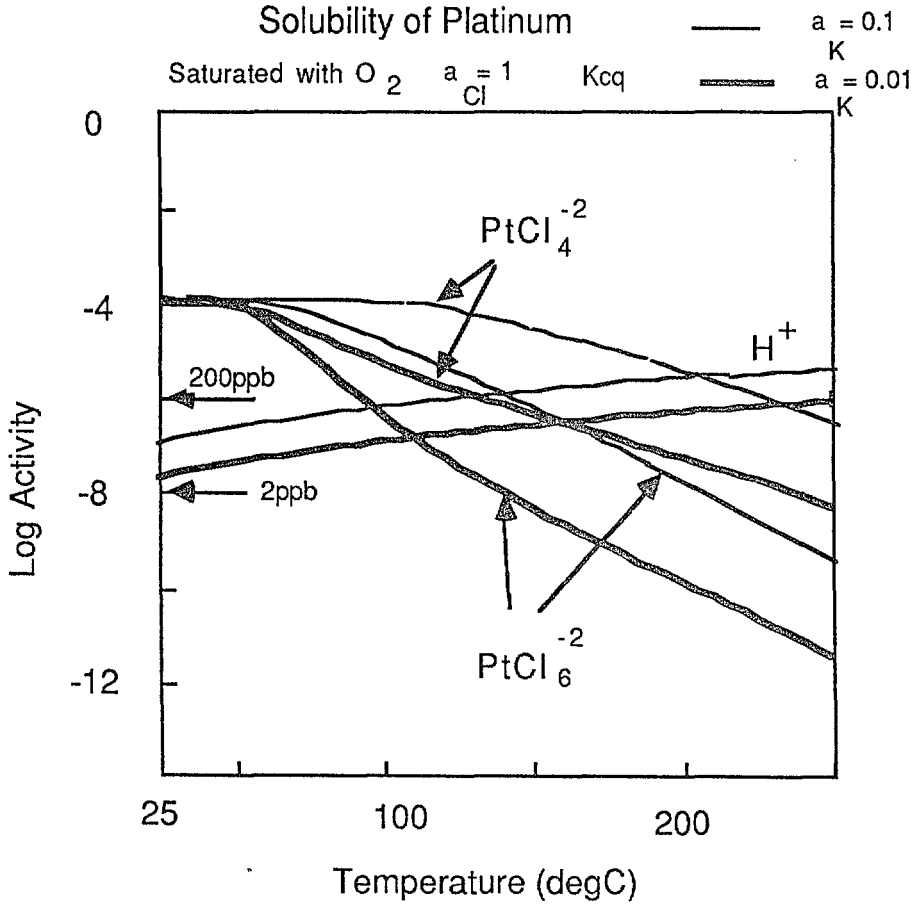

Fig. 10. Diagram showing variation in the solubility of platinum (as log activity of aqueous species) with temperature in a fluid saturated with atmospheric oxygen and buffered by the Kcq(potash-feldspar+kaolinite+quartz) assemblage. Numbers near the left ordinate axis represent approximate metal concentration. $a_{\text{total dissolved N}} = 1$, $a_{Cl^-} = 1$, $a_{K^+} = 0.1$ and 0.01.

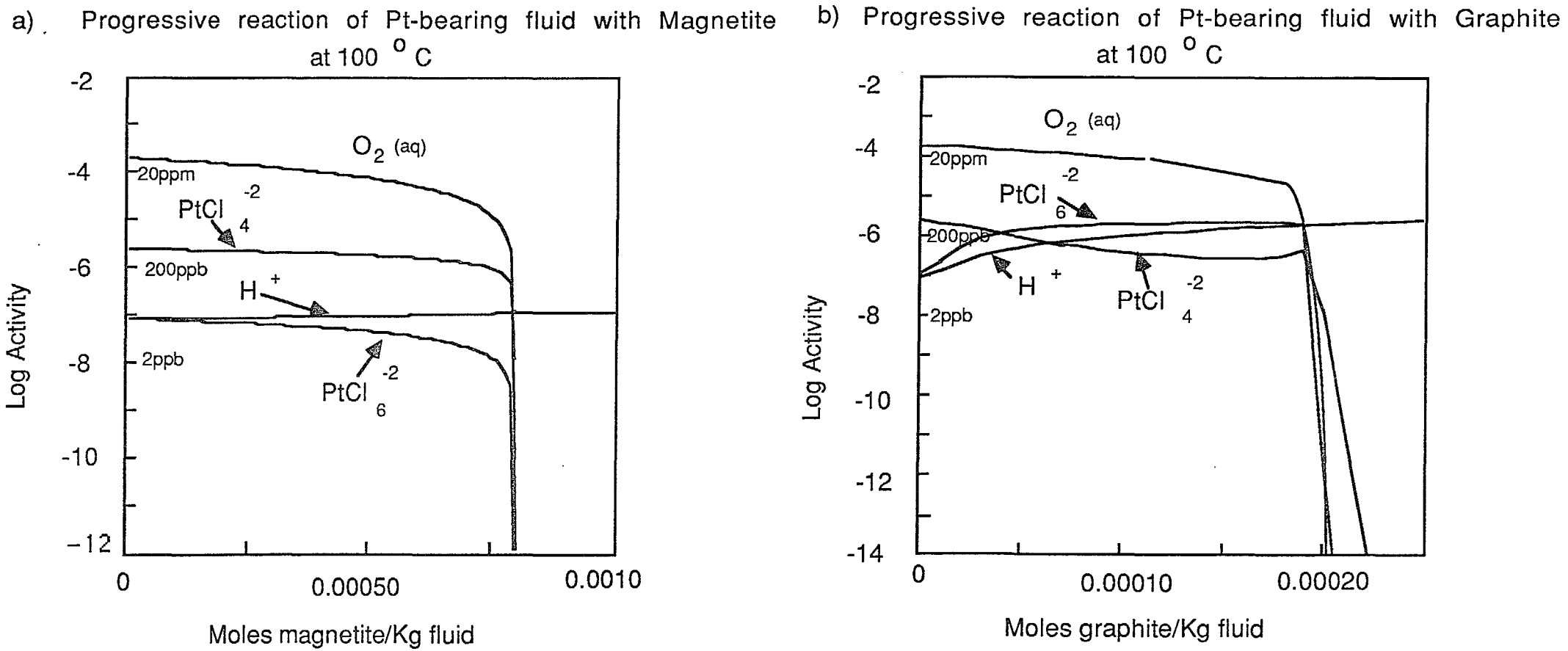

Fig. 11. Diagram showing drop in the activity of aqueous species of platinum as a saline ($a_{Cl^-} = 1$) fluid buffered by the Kmq assemblage($a_{K^+} = 0.01$) starts reacting with a) magnetite and b) graphite at 100°C. Numbers near the left ordinate axis represent approximate metal concentration.

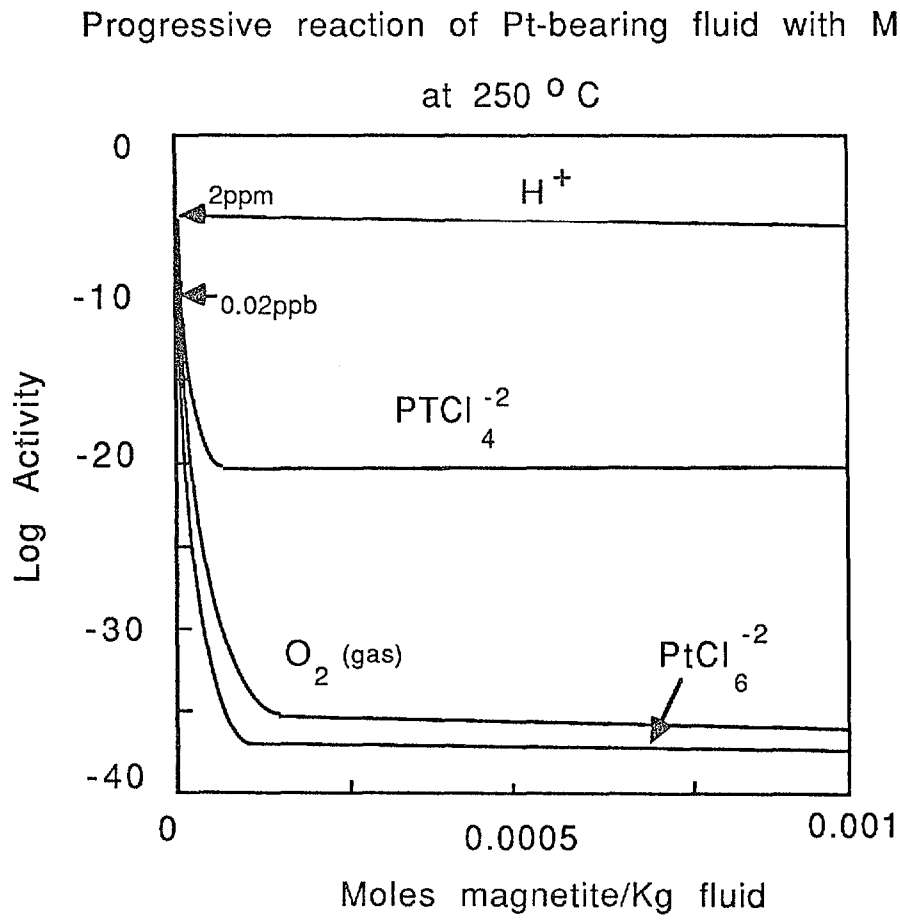

Fig. 12. Diagram showing changes in the activity of aqueous species of platinum as saline (a_{Cl^-} = 2), fluid buffered by the Mn_3O_4+Mn_2O_3 and Kmq (a_{K^+} =1)assemblages starts reacting with magnetite at 250°C. Numbers near the left ordinate axis represent approximate metal concentration.

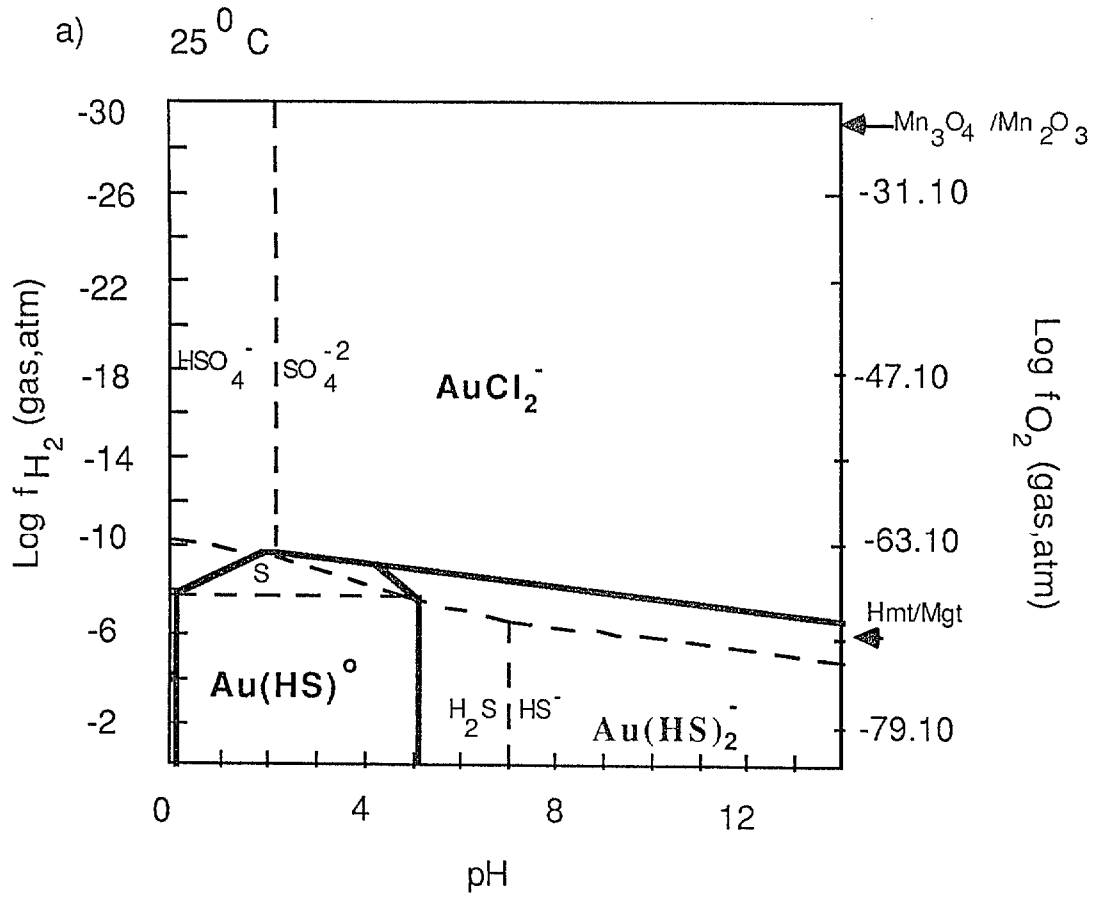
a)
25 0 C
-30
-26
-22
-18
-14
-10
-6
-2
Log f H2 (gas,atm)
HSO4-
SO4-2
AuCl2-
S
Au(HS)°
H2S
HS-
Au(HS)2-
Mn3O4 /Mn2O3
-31.10
-47.10
-63.10
Hmt/Mgt
-79.10
Log fO2 (gas,atm)
0
4
8
12
pH

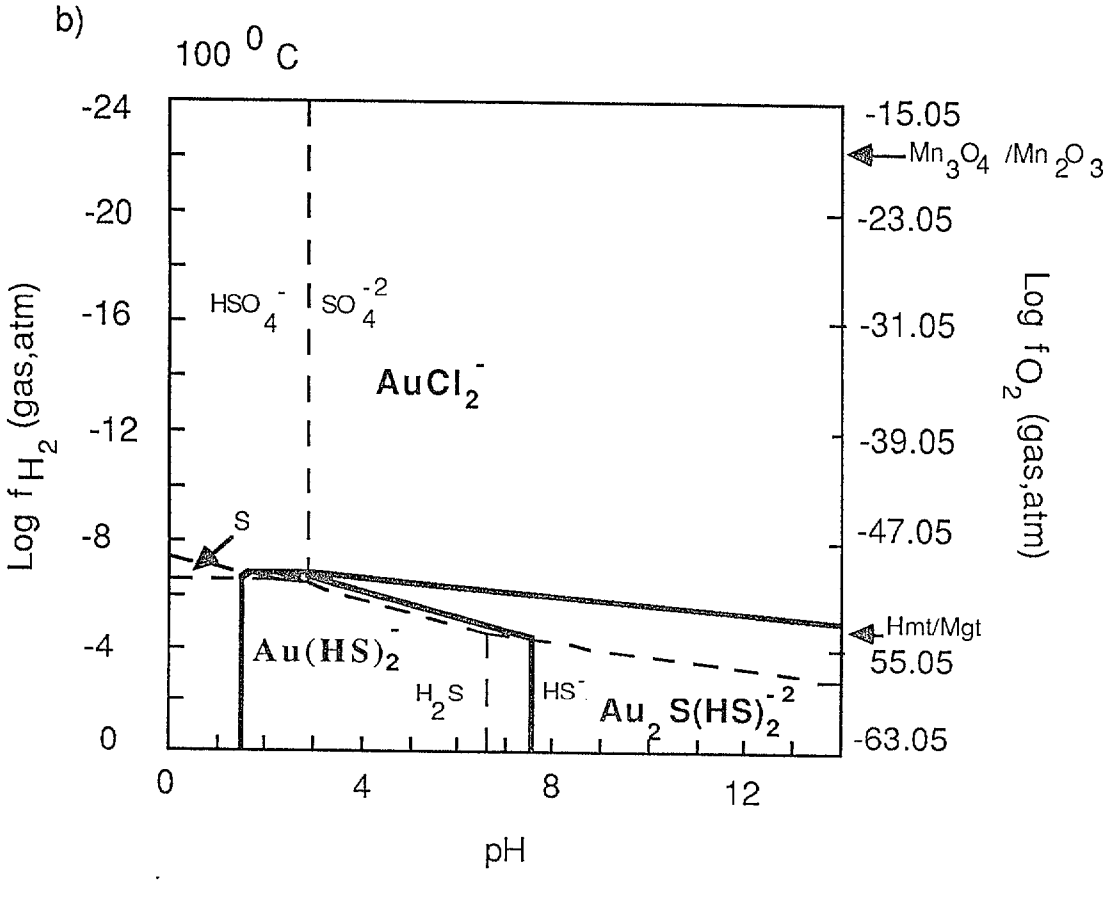
b)
100 0 C
-24
-20
-16
-12
-8
-4
0
Log f H2 (gas,atm)
HSO4-
SO4-2
AuCl2-
S
Au(HS)2-
H2S
HS-
Au2S(HS)2-2
-15.05
Mn3O4 /Mn2O3
-23.05
-31.05
-39.05
-47.05
Hmt/Mgt
55.05
-63.05
Log fO2 (gas,atm)
0
4
8
12
pH

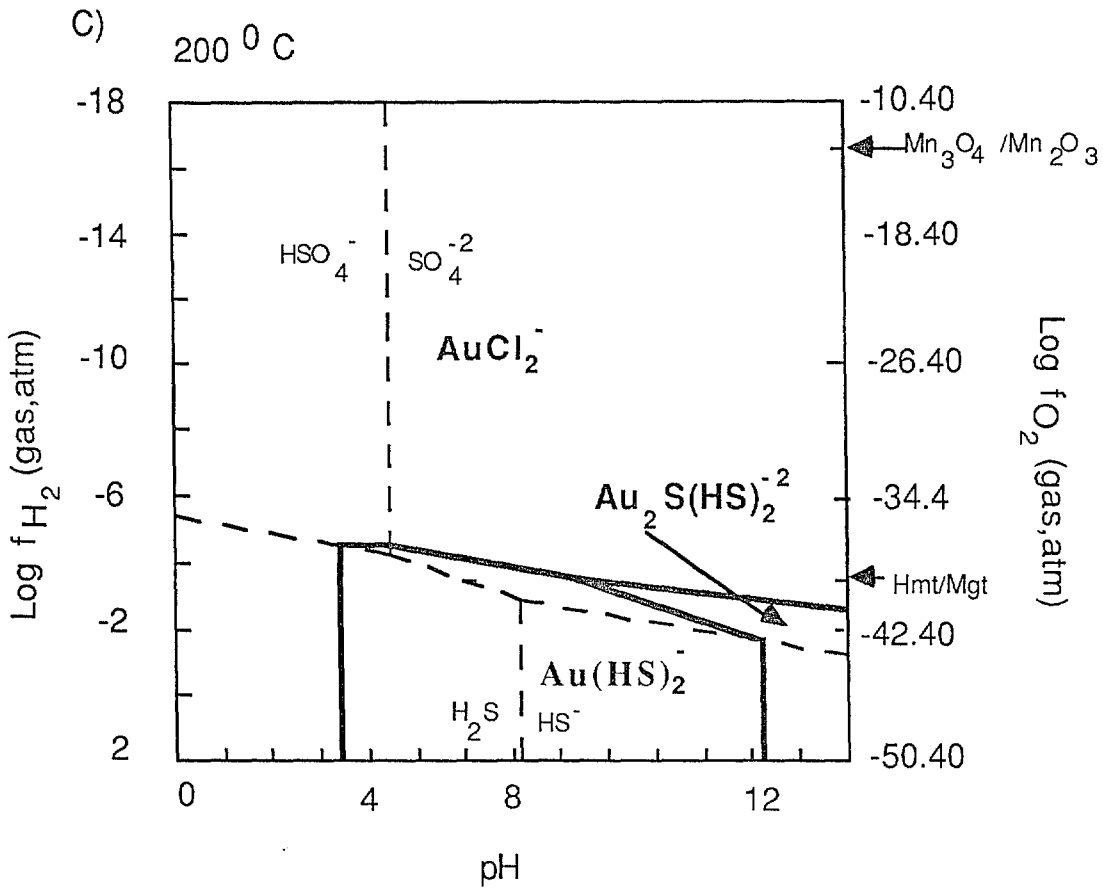

Fig. 13. Log f_{H_2} - pH diagrams showing the stability fields of aqueous species of gold. Also shown along the right ordinate axis are the corresponding Log f_{O_2} values. Calculations have been made for $a_{Cl^-} = 2$, $a_{\text{dissolved S}} = 0.001$. Dashed lines denote the stability fields of aqueous species of sulfur, while solid lines denote the stability fields of aqueous species of gold. The system is undersaturated with solid gold. Arrows on the right ordinate axis indicate positions of Hmt/Mgt (hematite+magnetite) and Mn_3O_4+Mn_2O_3 redox buffer assemblages. keeping in view the experimental data of Renders and Seward(1988) on the solubility of gold at 25°C, at 25°C $Au_2S(HS)_2^{-2}$ has not been included in the sytem, instead Au(HS)° has been added. At higher temperatures, $Au_2S(HS)_2^{-2}$ has been considered while Au(HS)° has been left out, due to the lack of stability data for this complex at higher temperatures . a - 25°C, b - 100°C, c - 200°C.

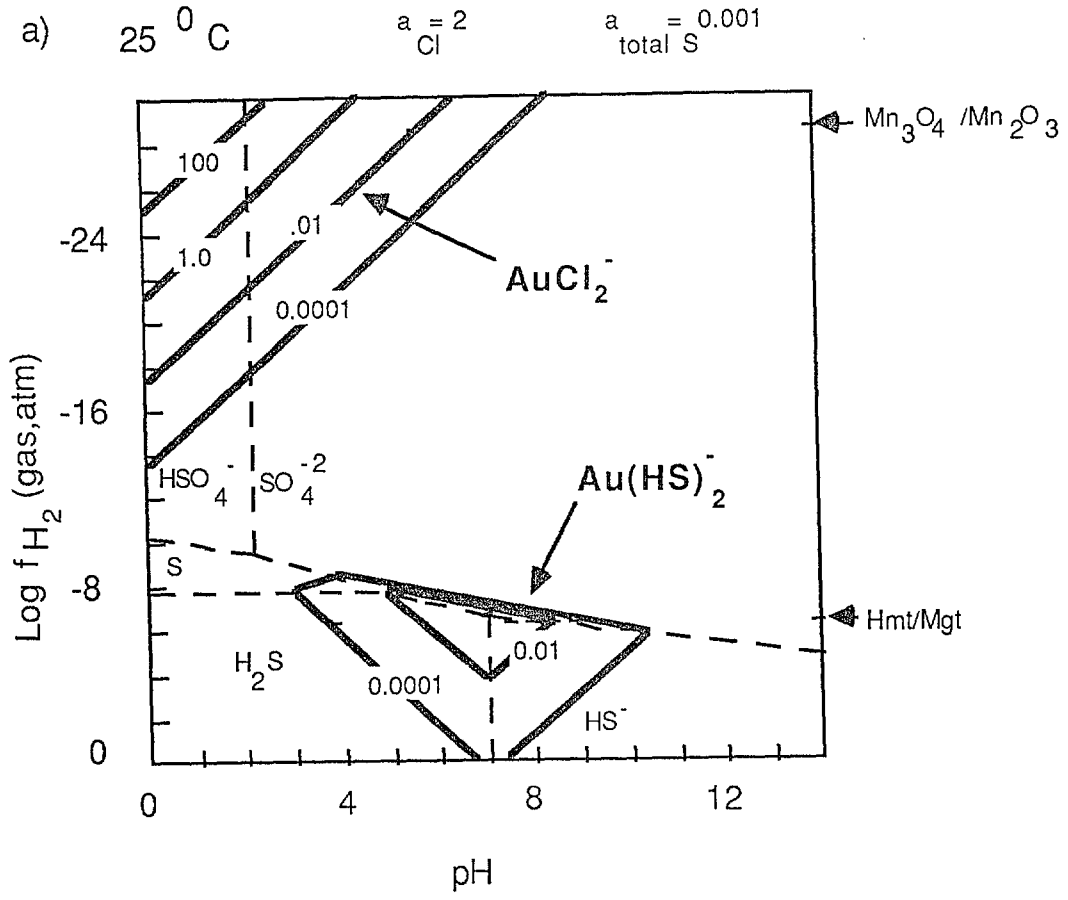
a) 25 0 C
a Cl = 2
a total S = 0.001
Mn3O4 /Mn2O3
100
1.0
.01
0.0001
AuCl2-
-24
-16
-8
0
HSO4-
SO4-2
Au(HS)2-
S
H2S
0.0001
0.01
HS-
Hmt/Mgt
Log f H2 (gas,atm)
0
4
8
12
pH

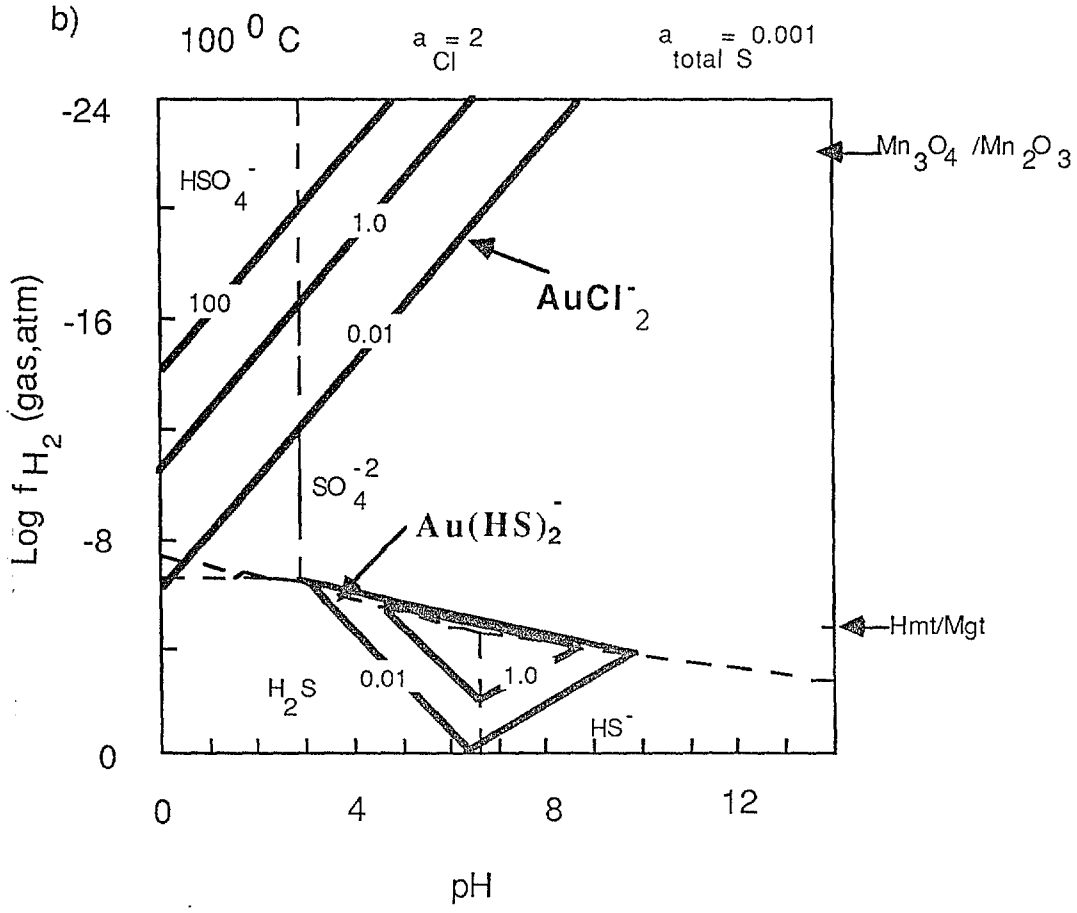
b) 100 0 C
a Cl = 2
a total S = 0.001
Mn3O4 /Mn2O3
HSO4-
1.0
100
0.01
AuCl-2
-24
-16
-8
0
SO4-2
Au(HS)2-
H2S
0.01
1.0
HS-
Hmt/Mgt
Log f H2 (gas,atm)
0
4
8
12
pH

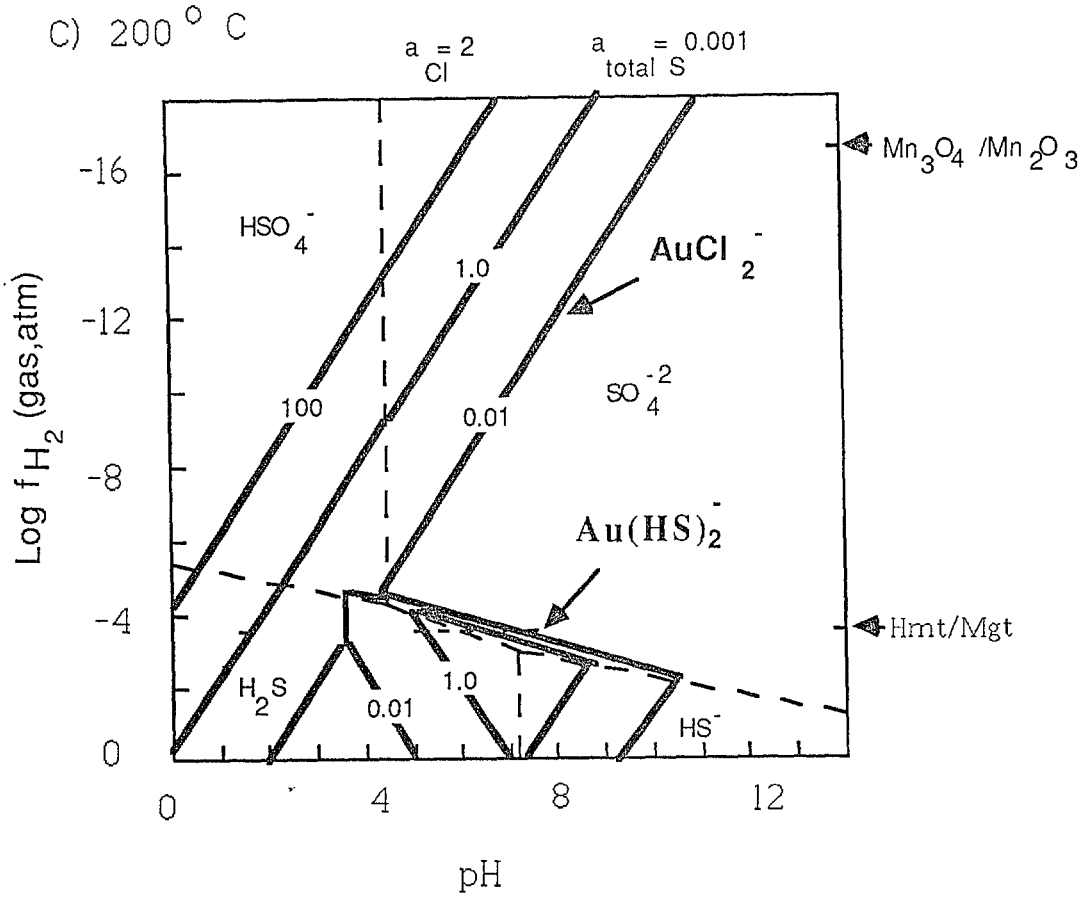

Fig. 14. Log f_{H_2} - pH diagrams showing the stability fields of solid gold along with the solubility contours of dissolved gold. Calculations have been made for $a_{Cl^-} = 2$, $a_{\text{dissolved S}} = 0.001$. Dashed lines denote the stability fields of aqueous species of sulfur, while solid lines denote the solubility contours in ppb of gold. Arrows on the right ordinate axis indicate positions of Hmt/Mgt (hematite+magnetite) and $Mn_3O_4+Mn_2O_3$ redox buffer assemblages. keeping in view the experimental data of Renders and Seward(1987) on the solubility of gold at 25°C, at 25°C $Au_2S(HS)_2^{-2}$ has not been included in the sytem, instead $Au(HS)^\circ$ has been added. At higher temperatures, $Au_2S(HS)_2^{-2}$ has been considered while $Au(HS)^\circ$ has been left out, due to the lack of stability data for this complex at higher temperatures . a - 25°C, b - 100°C, c - 200°C.

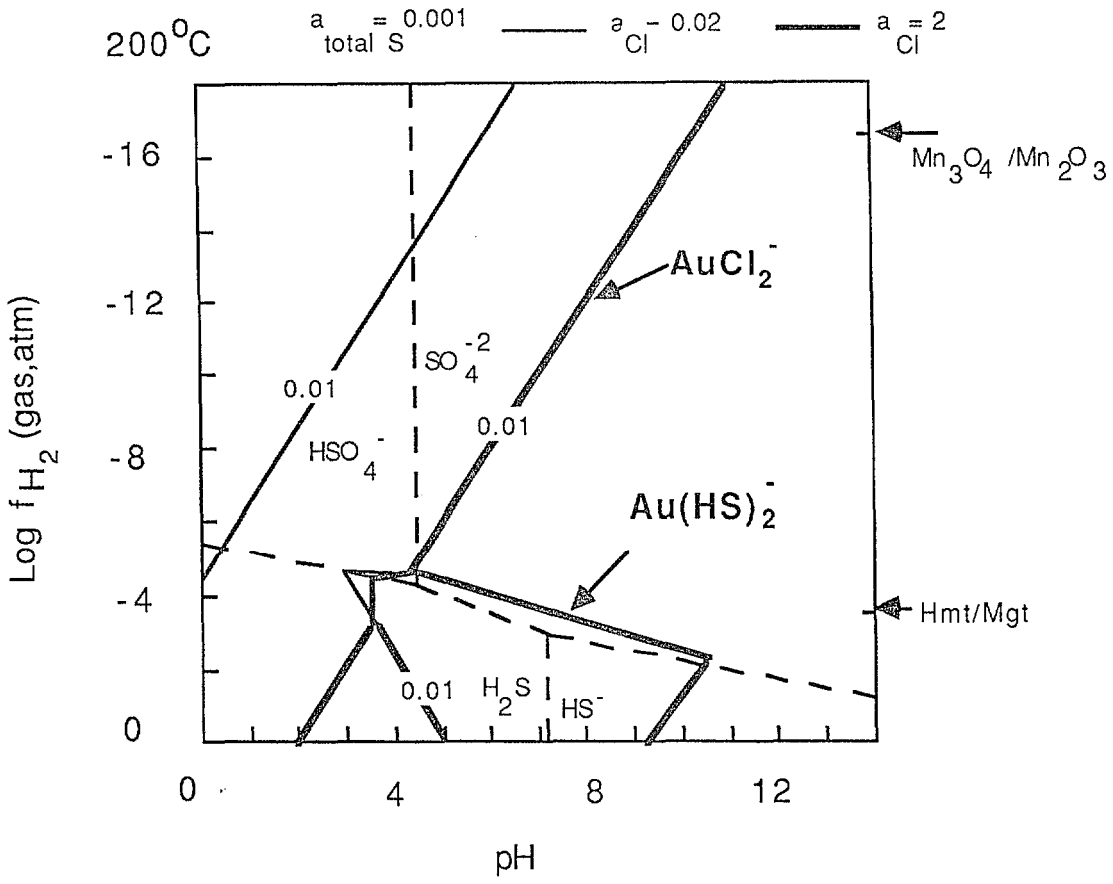

Fig. 15. Log f_{H_2} - pH diagram at 200°C showing the effect of change in the activity of total chloride in the fluid on the solubility of gold. $a_{\text{total dissolved S}}$ = 0.001. Dashed lines denote the stability fields of aqueous species of sulfur. Solubility contours of 0.01 ppb of gold have been drawn for a_{Cl^-} = 2(solid thick line) and 0.02(solid thin line). Arrows on the right ordinate axis indicate positions of Hmt/Mgt (hematite+magnetite) and Mn_3O_4+Mn_2O_3 redox buffer assemblages.

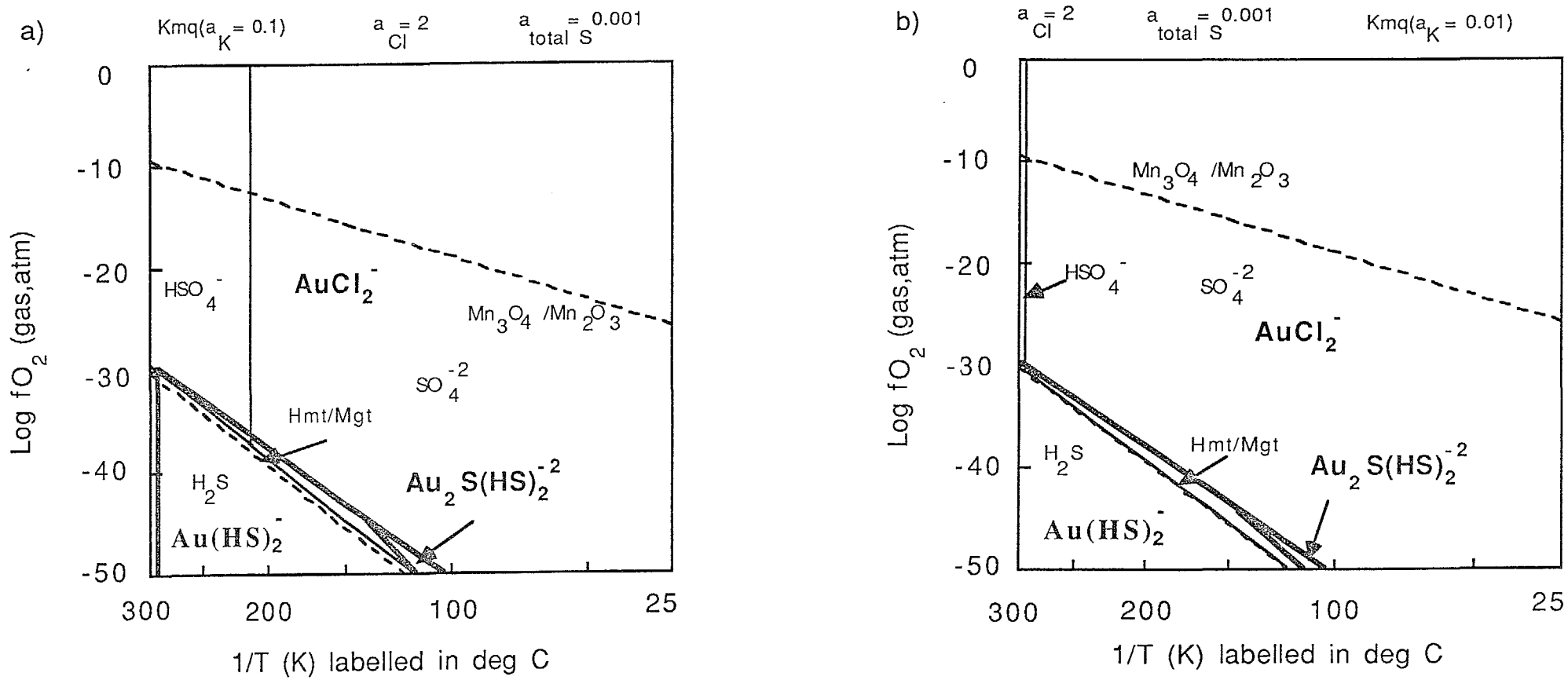

Fig. 16. Log f_{O2} - 1/T diagrams showing the stability fields of aqueous species of gold in a system buffered by the Kmq assemblage. Calculations have been done for $a_{Cl^-} = 2$ and $a_{total\ dissolved\ s} = 0.001$. Dashed lines denote boundaries between the aqueous speceies of sulfur. Solid lines denote the stability fields of aqueous species of gold. The system is undersaturated with solid gold. Dashed lines represent the Mn_3O_4+Mn_2O_3 and magnetite+hematite redox buffer assemblages. a - a_{K^+} =0.1, b - a_{K^+} = 0.01

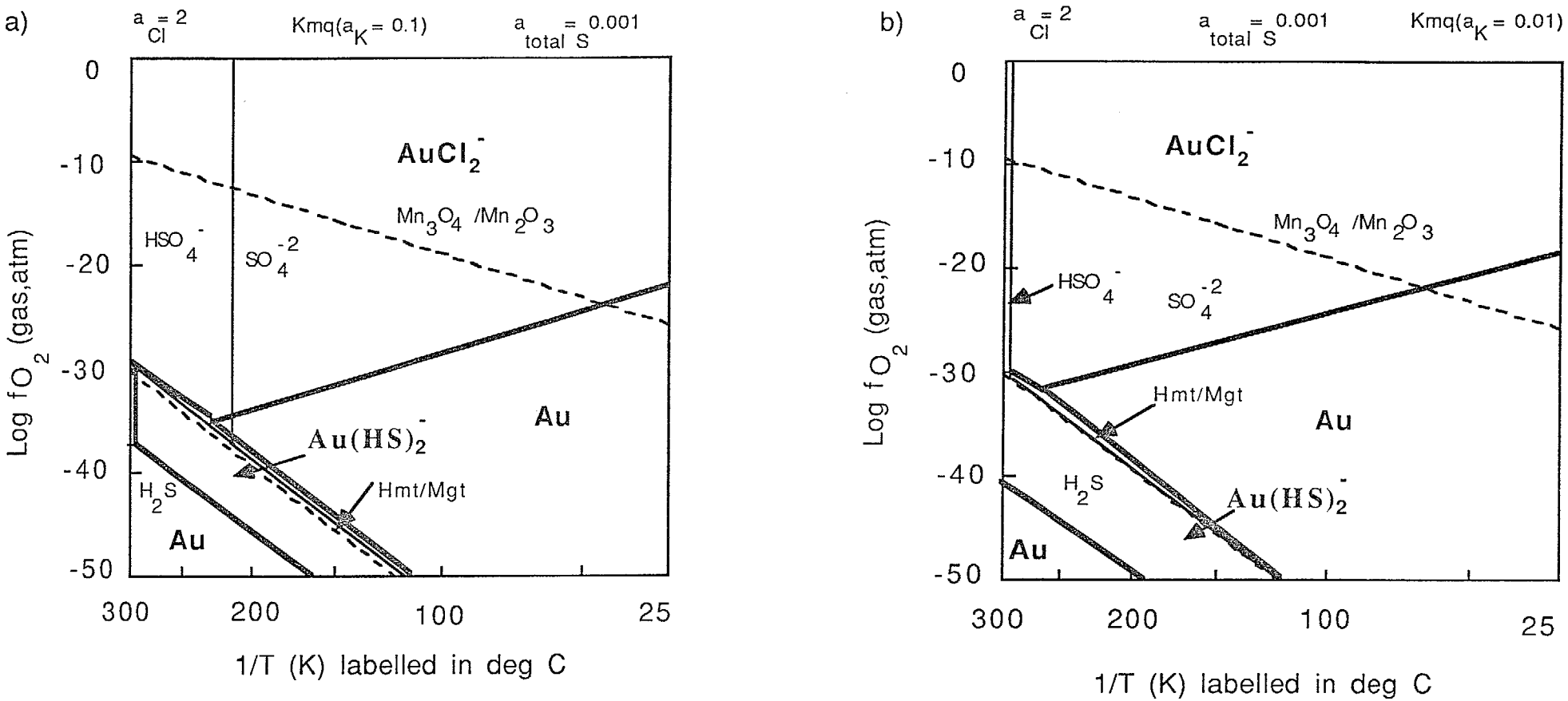

Fig. 17. Log f_{O2}- 1/T diagrams showing the stability fields the aqueous specis of gold in a system saturated with solid gold and buffered by the Kmq assemblage. Calculations have been done for $a_{Cl^-} = 2$ and $a_{total\ dissolved\ S} = 0.001$ Dashed lines denote boundaries between the aqueous speceies of sulfur. Solid lines represent boundaries between solid gold and the aqueous species of gold calculated for 0.01 ppb of dissolved gold. Dashed lines represent the Mn_3O_4+Mn_2O_3 and magnetite+hematite redox buffer assemblages. a - $a_{K^+} = 0.1$, b - $a_{K^+} = 0.01$

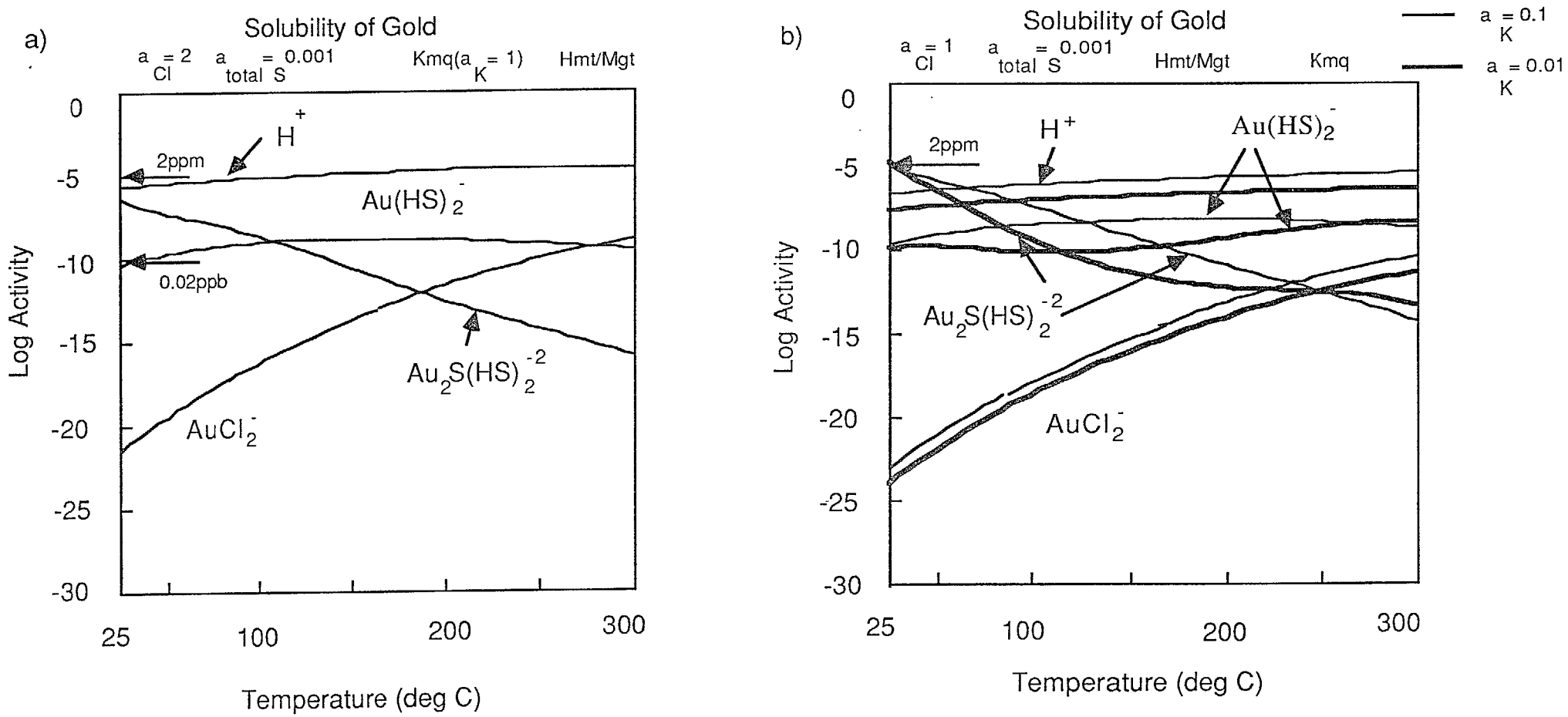

Fig. 18. Diagram showing variation in the solubility of gold(as log activity of aqueous species) with temperature in a fluid buffered by the Kmq and Hmt/Mgt (magnetite+hematite)assemblages. Numbers near the left ordinate axis represent approximate metal concentration. $a_{\text{total dissolved S}} = 0.001$, a - $a_{Cl^-} = 2$, $a_{K^+} = 1$, b - $a_{Cl^-} = 1$, $a_{K^+} = 0.1$, c - $a_{Cl^-} = 1$, $a_{K^+} = 0.01$

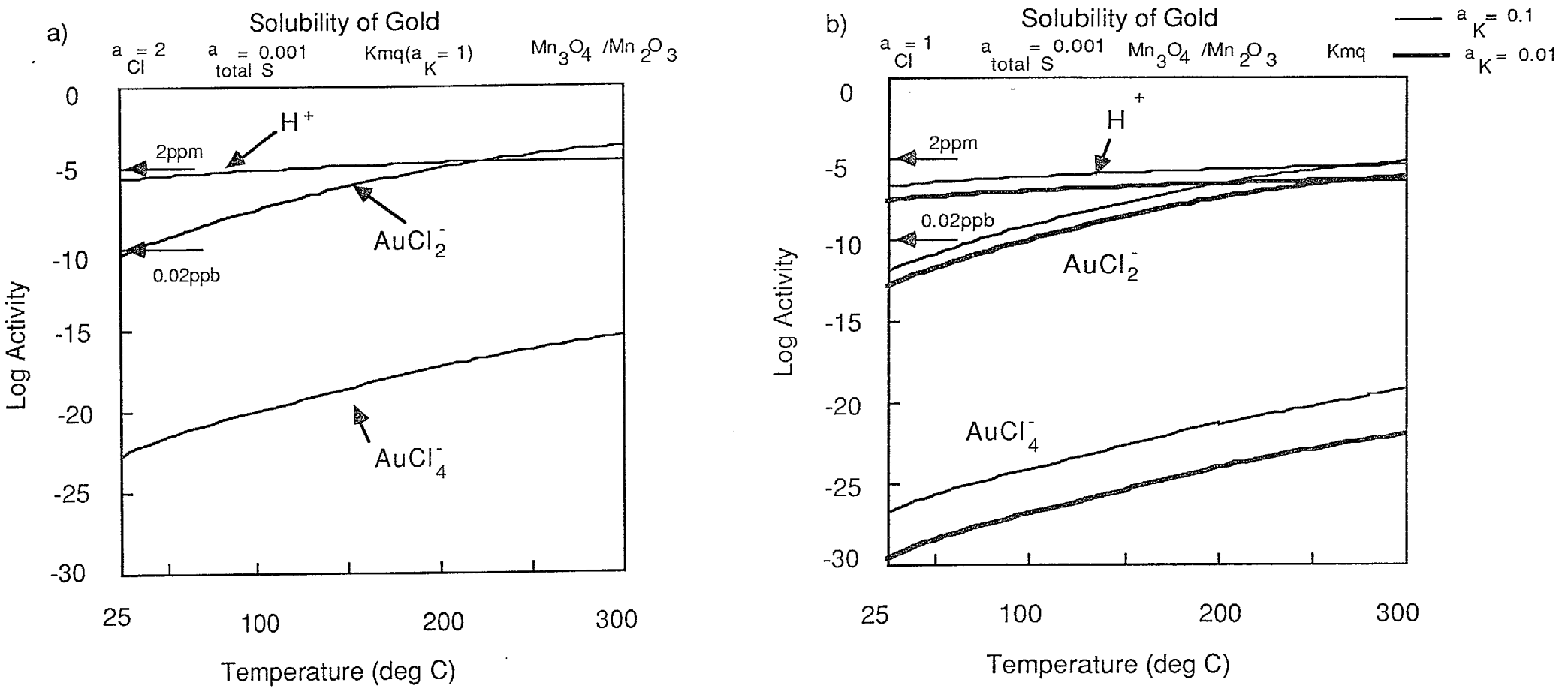

Fig. 19. Diagram showing variation in the solubility of gold(as log activity of aqueous species) with temperature in a fluid buffered by the Kmq and Mn_3O_4+Mn_2O_3 assemblages. Numbers near the left ordinate axis represent approximate metal concentration. $a_{\text{total dissolved S}} = 0.001$, a - $a_{Cl^-} = 2$, $a_{K^+} = 1$, b - $a_{Cl^-} = 1$, $a_{K^+} = 0.1$, c - $a_{Cl^-} = 1$, $a_{K^+} = 0.01$

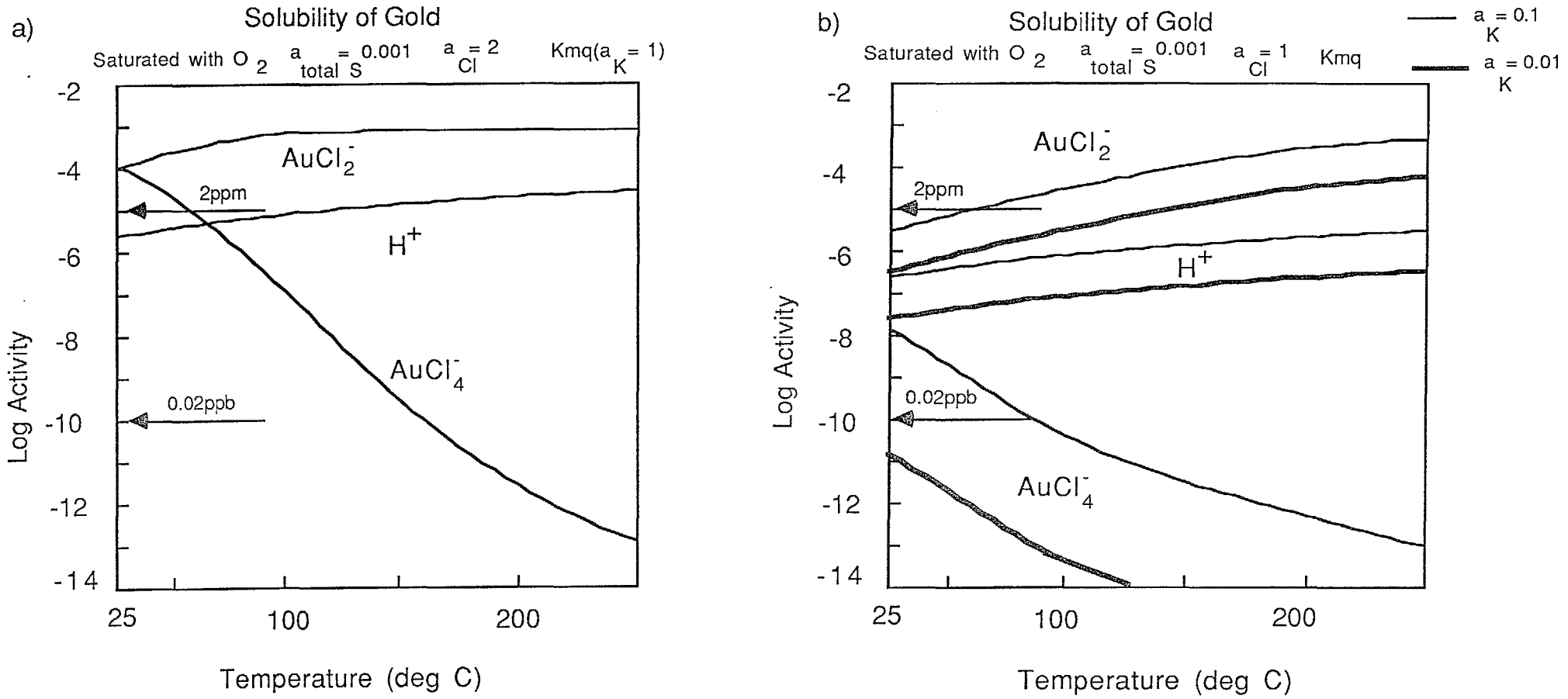

Fig. 20. Diagram showing variation in the solubility of gold (as log activity of aqueous species) with temperature in a fluid saturated with atmospheric oxygen and buffered by the Kmq assemblage. Numbers near the left ordinate axis represent approximate metal concentration. $a_{\text{total dissolved S}} = 0.001$, a - a_{Cl^-} = 2m, $a_{K^+} = 1$, b - $a_{Cl^-} = 1$, $a_{K^+} = 0.1$ and 0.01

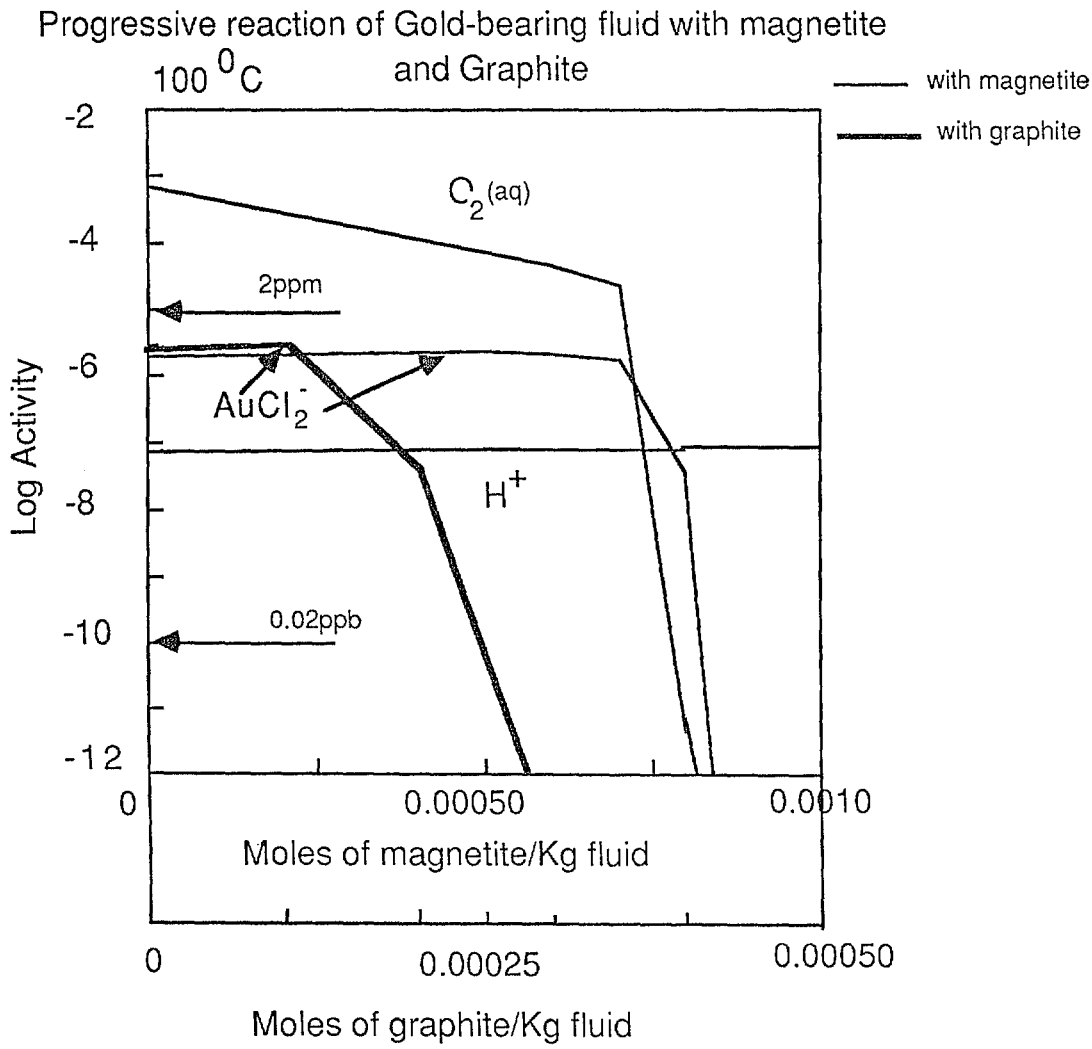

Fig. 21. Diagram showing drop in the activity of aqueous species of gold as a saline (a_{Cl^-} = 1) fluid buffered by the Kmq assemblage(a_{K^+} = 0.01) starts reacting with magnetite(solid thin lines) and graphite(solid thick line) at 100°C. Numbers near the left ordinate axis represent approximate metal concentration.